Intrusive acceleration strategies for Uncertainty Quantification

Jonas Kusch[a], Jannick Wolters[b], Martin Frank[c]

[a]*Karlsruhe Institute of Technology, Karlsruhe, jonas.kusch@kit.edu*

[b]*Karlsruhe Institute of Technology, Karlsruhe, jannick.wolters@kit.edu*

[c]*Karlsruhe Institute of Technology, Karlsruhe, martin.frank@kit.edu*

Abstract

Methods for quantifying the effects of uncertainties in hyperbolic problems can be divided into intrusive and non-intrusive techniques. Non-intrusive methods allow using a given deterministic solver as a black box while being embarrassingly parallel. Intrusive methods on the other hand do not suffer from aliasing effects and provide a more general framework for adaptive refinement techniques. Since the moment system solved by intrusive methods is not necessarily hyperbolic, the Intrusive Polynomial Moment (IPM) method has been introduced. IPM maintains hyperbolicity but comes at the cost of having to solve an optimization problem in every spatial cell and every time step. In this work, we propose acceleration techniques for intrusive methods. When solving steady problems, the numerical costs arising from repeatedly solving the IPM optimization problem can be reduced by borrowing ideas from shape optimization. Integrating the iteration to solve the optimization problem into the moment update guarantees local convergence while reducing numerical costs. Furthermore, we propose to use non-intrusive methods as a preconditioner for intrusive methods. Consequently, a large amount of iterations to the steady solution are performed by a cheap method, while maintaining the increased accuracy of an intrusive method. Additionally, we propose an adaptive implementation of the IPM method, which further reduces numerical costs. We demonstrate the effectiveness of the proposed strategies by comparing results of the uncertain NACA0012 testcase as well as a bent shock tube experiment with non-intrusive methods.

Keywords: uncertainty quantification, conservation laws, hyperbolic, intrusive, stochastic-Galerkin, Collocation, Intrusive Polynomial Moment Method

1. Introduction

Hyperbolic equations play an important role in various research areas such as fluid dynamics or plasma physics. Efficient numerical methods combined with robust implementations are available for these problems, however they do not account for uncertainties which can arise in measurement data or modeling assumptions. Including the effects of uncertainties in differential equations has become an important topic in the last decades.

Commonly, methods to quantify uncertainties use a polynomial chaos (PC) expansion [1, 2] to represent the solution, i.e. the uncertain space is spanned by polynomial basis functions. The remaining task is then to determine adequate expansion coefficients, often called moments or PC coefficients. Numerical methods for approximating these coefficients can be divided into intrusive and non-intrusive techniques. A popular non-intrusive method is the stochastic-Collocation (SC) method, see e.g. [3, 4, 5], which computes the moments with the help of a numerical quadrature rule. Commonly, SC uses sparse grids, since they posses a reduced number of collocation points for multi-dimensional problems. Since the solution at a fixed quadrature point can be computed by a standard deterministic solver, the SC method does not require a significant

implementation effort. Furthermore, SC is embarrassingly parallel, since the required computations can be carried out simultaneously on different cores.

The main idea of intrusive methods is to derive a system of equations describing the time evolution of the moments which can then be solved with a deterministic numerical scheme. A popular approach to describe the moment system is the stochastic-Galerkin (SG) method [6], which chooses a polynomial solution ansatz and performs a Galerkin projection to derive a closed system of equations. One significant drawback of SG is its not necessarily hyperbolic moment system [7]. A generalization of stochastic-Galerkin, which ensures hyperbolicity is the Intrusive Polynomial Moment (IPM) method [7]. Instead of performing the PC expansion on the solution, the IPM method represents the entropy variables with polynomials. Besides yielding a hyperbolic moment system, the IPM method has several advantages: Choosing a quadratic entropy yields the stochastic-Galerkin moment system, i.e. IPM generalizes different intrusive methods. Furthermore, at least for scalar problems, IPM is significantly less oscillatory compared to SG [8]. Also, as discussed in [7], when choosing a physically correct entropy of the deterministic problem, the IPM solution dissipates the expectation value of the entropy, i.e. the IPM method yields a physically correct entropy solution. Unfortunately, the desirable properties of IPM come along with significantly increased numerical costs, since IPM requires the repeated computation of the entropic expansion coefficients from the moment vector, which involves solving a convex optimization problem. However, IPM and minimal entropy methods in general are well suited for modern HPC architectures, which can be used to reduce the run time [9].

When studying hyperbolic equations, the moment approximations of various methods such as Stochastic Galerkin [10], IPM [11] and stochastic-Collocation [12, 13] tend to show incorrect discontinuities in certain regions of the physical space. These non-physical structures dissolve when the number of basis functions is increased [14, 15] or when artificial diffusion is added through the spatial numerical method [15] or filters [11]. Also, a multi-element approach which divides the uncertain domain into cells and uses piece-wise polynomial basis functions to represent the solution has proven to mitigate non-physical discontinuities [16, 17]. These structures commonly arise on a small portion of the space-time domain. Therefore, intrusive methods seem to be an adequate choice since they are well suited for adaptive strategies. By locally increasing the polynomial order [18, 19, 20] or adding artificial viscosity [11] at certain spatial positions and time steps in which complex structures such as discontinuities occur, a given accuracy can be reached with significantly reduced numerical costs. In addition to that, the number of moments needed to obtain a certain order with intrusive methods is asymptotically smaller than the number of quadrature points for SC. An additional downside of collocation methods are aliasing effects, which stem from the inexact approximation of integrals. Consequently, collocation methods typically require a higher number of unknowns than intrusive methods to reach a given accuracy [21, 22]. Therefore, one aim should be to accelerate intrusive methods, since they can potentially outperform non-intrusive methods in complex and high-dimensional settings.

In this paper, we propose acceleration techniques for intrusive methods and compare them against stochastic-Collocation. For steady and unsteady problems, we use adaptivity:

- The intrusive nature of SG and IPM can be used to locally increase the number of moments whenever the solution has a complex structure in the random variable (as well as decrease the number of moments if not). To guarantee an efficient implementation, we propose an adaptive discretization strategy for IPM.

A steady problem provides different opportunities to take advantage of features of intrusive methods:

- When using adaptivity, one can perform a large number of iterations to the steady state solution on a low number of moments and increase the maximal truncation order when the distance to the steady state has reached a specified barrier. Consequently, a large number of iterations will be performed by a cheap, low order method, i.e. we can reduce numerical costs.
- Accelerate the convergence to the steady state IPM solution by applying IPM as a post-processing step for collocation methods: We converge the moments of the solution to a steady state with an

inaccurate, but cheap collocation method and then use the resulting collocation moments as starting values for an expensive but accurate intrusive method such as IPM, which we then again converge to steady state.

- Perform an inexact map from the moments to the entropic expansion coefficients for IPM: Since the moments during the iteration process are inaccurate, i.e. they are not the correct steady state solution, we propose to not fully converge the dual iteration, which solves the IPM optimization problem. Consequently, the entropic expansion coefficients and the moments are converged simultaneously to their steady state, which is similar to the idea of one-shot optimization in shape optimization [23].

The effectiveness of these acceleration ideas are tested by comparing results with stochastic-Collocation for the uncertain NACA test case as well as a bent shock tube problem. Our numerical studies show the following main results:

- In our test cases, the need to solve an optimization problem when using the IPM method leads to a significantly higher run time than SC and SG. However when using the discussed acceleration techniques, IPM requires the shortest time to reach a given accuracy.
- Comparing SG with IPM, one observes that for the same number of unknowns, SG yields more accurate expectation values, whereas IPM shows improved variance approximations.
- By studying aliasing effects, we show that SC requires a higher number of unknowns than intrusive methods (even for one spatial dimension) to reach the same accuracy level.
- Using sparse grids for the IPM discretization when the space of uncertainty is multi-dimensional, the number of quadrature points needed to guarantee sufficient regularity of the Hessian matrix is significantly increased.

The IPM and SG calculations use a semi-intrusive numerical method, meaning that the discretization allows recycling a given deterministic code to generate the IPM solver. While facilitating the task of implementing general intrusive methods, this framework allows a fair comparison of intrusive and non-intrusive methods, since the intrusive method can be based on the same deterministic code as the code used in a black-box fashion for stochastic-Collocation.

The paper is structured as follows: After the introduction, we present the discussed methods in more detail in section 2. The numerical discretization as well as the implementation and structure of the semi-intrusive method is introduced in section 3. Section 4.1 discusses the IPM acceleration with a non-intrusive method and in section 4.2, we discuss the idea of not converging the dual iteration. Section 5 extends the presented numerical framework to an algorithm making use of adaptivity. A comparison of results computed with the presented methods is then given in section 7, followed by a summary and outlook in section 8.

2. Background

In the following, we briefly introduce the notation and methods used in this work. A general hyperbolic set of equations with random initial data can be written as

$$\partial_t \boldsymbol{u}(t,\boldsymbol{x},\boldsymbol{\xi}) + \nabla \cdot \boldsymbol{f}(\boldsymbol{u}(t,\boldsymbol{x},\boldsymbol{\xi})) = \boldsymbol{0} \quad \text{in } D, \tag{1a}$$

$$\boldsymbol{u}(t=0,\boldsymbol{x},\boldsymbol{\xi}) = \boldsymbol{u}_{\mathrm{IC}}(\boldsymbol{x},\boldsymbol{\xi}), \tag{1b}$$

where the solution $\boldsymbol{u} \in \mathbb{R}^p$ depends on time $t \in \mathbb{R}^+$, spatial position $\boldsymbol{x} \in D \subseteq \mathbb{R}^d$ as well as a vector of random variables $\boldsymbol{\xi} \in \Theta \subseteq \mathbb{R}^s$ with given probability density functions $f_{\Xi,i}(\xi_i)$ for $i = 1, \cdots, s$. Hence, the probability density function of $\boldsymbol{\xi}$ is $f_\Xi(\boldsymbol{\xi}) := \prod_{i=1}^s f_{\Xi,i}(\xi_i)$. The physical flux is given by $\boldsymbol{f} : \mathbb{R}^p \to \mathbb{R}^{d\times p}$. To simplify notation, we assume that only the initial condition is random, i.e. $\boldsymbol{\xi}$ enters through the definition of $\boldsymbol{u}_{IC}$. Equations (1) are usually supplemented with boundary conditions, which we will specify later for the individual problems.

Due to the randomness of the solution, one is interested in determining the expectation value or the variance, i.e.

$$\mathrm{E}[\boldsymbol{u}] = \langle \boldsymbol{u} \rangle, \qquad \mathrm{Var}[\boldsymbol{u}] = \langle (\boldsymbol{u} - \mathrm{E}[\boldsymbol{u}])^2 \rangle,$$

where we use the bracket operator $\langle \cdot \rangle := \int_\Theta \cdot f_\Xi(\boldsymbol{\xi}) d\xi_1 \cdots d\xi_s$. To approximate quantities of interest (such as expectation value, variance or higher order moments), the solution is spanned with a set of polynomial basis functions $\varphi_i : \Theta \to \mathbb{R}$ such that for the multi-index $i = (i_1, \cdots, i_s)$ we have $|i| \leq M$. Note that this yields

$$N := \binom{M+s}{s} \tag{2}$$

basis functions when defining $|i| := \sum_{n=1}^s |i_n|$. Commonly, these functions are chosen to be orthonormal polynomials [1] with respect to the probability function, i.e. $\langle \varphi_i \varphi_j \rangle = \prod_{n=1}^s \delta_{i_n j_n}$. The generalized polynomial chaos (gPC) expansion [2] approximates the solution by

$$\mathcal{U}(\hat{\boldsymbol{u}}; \boldsymbol{\xi}) := \sum_{|i| \leq M} \hat{\boldsymbol{u}}_i \varphi_i(\boldsymbol{\xi}) = \hat{\boldsymbol{u}}^T \boldsymbol{\varphi}(\boldsymbol{\xi}), \tag{3}$$

where the deterministic expansion coefficients $\hat{\boldsymbol{u}}_i \in \mathbb{R}^p$ are called moments. To allow a more compact notation, we collect the N moments for which $|i| \leq M$ holds in the moment matrix $\hat{\boldsymbol{u}} := (\hat{\boldsymbol{u}}_i)_{|i| \leq M} \in \mathbb{R}^{N \times p}$ and the corresponding basis functions in $\boldsymbol{\varphi} := (\varphi_i)_{|i| \leq M} \in \mathbb{R}^N$. In the following, the dependency of $\mathcal{U}$ on $\boldsymbol{\xi}$ will occasionally be omitted for sake of readability. The solution ansatz (3) is L^2 optimal if the moments are chosen to be the Fourier coefficients $\hat{\boldsymbol{u}}_i \equiv \langle \boldsymbol{u} \varphi_i \rangle \in \mathbb{R}^p$. One can use the solution ansatz (3) to compute the quantities of interest. Indeed, we have that

$$\mathrm{E}[\mathcal{U}(\hat{\boldsymbol{u}})] = \hat{\boldsymbol{u}}_0, \quad \mathrm{Var}[\mathcal{U}(\hat{\boldsymbol{u}})] = \mathrm{E}[\mathcal{U}(\hat{\boldsymbol{u}})^2] - \mathrm{E}[\mathcal{U}(\hat{\boldsymbol{u}})]^2 = \left(\sum_{i=1}^N \hat{u}_{\ell i}^2 \right)_{\ell = 1, \cdots, p}.$$

The core idea of the stochastic-Collocation method is to compute the moments in the gPC expansion with a quadrature rule. Given a set of Q quadrature weights w_k and quadrature points $\boldsymbol{\xi}_k$, the moments are approximated by

$$\hat{\boldsymbol{u}}_i = \langle \boldsymbol{u} \varphi_i \rangle \approx \sum_{k=1}^Q w_k \boldsymbol{u}(t, \boldsymbol{x}, \boldsymbol{\xi}_k) \varphi_i(\boldsymbol{\xi}_k) f_\Xi(\boldsymbol{\xi}_k).$$

Hence, the moments can be computed by running a given deterministic solver for the original problem at each quadrature point. To reduce numerical costs in multi-dimensional settings, SC commonly uses sparse grids as quadrature rule: While tensorized quadrature sets require $O(M^s)$ quadrature points to integrate polynomials of total degree M exactly, sparse grids only require $O(M(\log_2(M)^{s-1}))$ quadrature points.

Intrusive methods derive a system which directly describes the time evolution of the moments: Plugging the solution ansatz (3) into the set of equations (1) and projecting the resulting residual to zero yields the stochastic-Galerkin moment system

$$\partial_t \hat{\boldsymbol{u}}_i(t, \boldsymbol{x}) + \nabla \cdot \langle \boldsymbol{f}(\mathcal{U}(\hat{\boldsymbol{u}})) \varphi_i \rangle = \boldsymbol{0}, \tag{4a}$$

$$\hat{\boldsymbol{u}}_i(t = 0, \boldsymbol{x}) = \langle \boldsymbol{u}_{\mathrm{IC}}(\boldsymbol{x}, \cdot) \varphi_i \rangle, \tag{4b}$$

with $|i| \leq M$. As already mentioned, the SG moment system is not necessarily hyperbolic. To ensure hyperbolicity, the IPM method uses a solution ansatz which minimizes a given entropy under a moment

constraint instead of a polynomial expansion (3). For a given convex entropy $s : \mathbb{R}^p \to \mathbb{R}$ for the original problem (1), the IPM solution ansatz is given by

$$\mathcal{U}(\hat{\boldsymbol{u}}) = \arg\min_{\boldsymbol{u}} \langle s(\boldsymbol{u}) \rangle \quad \text{subject to } \hat{\boldsymbol{u}}_i = \langle \boldsymbol{u}\varphi_i \rangle \text{ for } |i| \leq M. \tag{5}$$

Rewritten in its dual form, (5) is transformed into an unconstrained optimization problem. Defining the variables $\boldsymbol{\lambda}_i \in \mathbb{R}^p$ where i is again a multi index, gives the unconstrained dual problem

$$\hat{\boldsymbol{\lambda}}(\hat{\boldsymbol{u}}) := \arg\min_{\boldsymbol{\lambda} \in \mathbb{R}^{N \times p}} \left\{ \langle s_*(\boldsymbol{\lambda}^T \boldsymbol{\varphi}) \rangle - \sum_{|i| \leq M} \boldsymbol{\lambda}_i^T \hat{\boldsymbol{u}}_i \right\}, \tag{6}$$

where $s_* : \mathbb{R}^p \to \mathbb{R}$ is the Legendre transformation of s, and $\hat{\boldsymbol{\lambda}} := (\hat{\boldsymbol{\lambda}}_i)_{|i| \leq M} \in \mathbb{R}^{N \times p}$ are called the dual variables. The solution to (5) is then given by

$$\mathcal{U}(\hat{\boldsymbol{u}}) = (\nabla_{\boldsymbol{u}} s)^{-1} (\hat{\boldsymbol{\lambda}}(\hat{\boldsymbol{u}})^T \boldsymbol{\varphi}). \tag{7}$$

When plugging this ansatz into the original equations (1) and projecting the resulting residual to zero again yields the moment system (4), but with the ansatz (7) instead of (3).

3. Discretization of the IPM system

3.1. Finite Volume Discretization

In the following, we discretize the moment system in space and time according to [8]. Due to the fact, that stochastic-Galerkin can be interpreted as IPM with a quadratic entropy, it suffices to only derive a discretization of the IPM moment system. Hence, we discretize the system (4) with the more general IPM solution ansatz (7). Omitting initial conditions and assuming a one-dimensional spatial domain, we can write the IPM system as

$$\partial_t \hat{\boldsymbol{u}} + \partial_x \boldsymbol{F}(\hat{\boldsymbol{u}}) = \boldsymbol{0}$$

with the flux $\boldsymbol{F} : \mathbb{R}^{N \times p} \to \mathbb{R}^{N \times p}$, $\boldsymbol{F}(\hat{\boldsymbol{u}}) = \langle \boldsymbol{f}(\mathcal{U}(\hat{\boldsymbol{u}}))\boldsymbol{\varphi}^T \rangle^T$. Due to hyperbolicity of the IPM moment system, one can use a finite-volume method to approximate the time evolution of the IPM moments. We choose the discrete unknowns which represent the solution to be the spatial averages over each cell at time t_n, given by

$$\hat{\boldsymbol{u}}_{ij}^n \simeq \frac{1}{\Delta x} \int_{x_{j-1/2}}^{x_{j+1/2}} \hat{\boldsymbol{u}}_i(t_n, x) dx.$$

If a moment vector in cell j at time t_n is denoted as $\hat{\boldsymbol{u}}_j^n = (\hat{\boldsymbol{u}}_{0j}^n, \cdots, \hat{\boldsymbol{u}}_{Nj}^n)^T \in \mathbb{R}^{N+1}$, the finite-volume scheme can be written in conservative form with the numerical flux $\boldsymbol{G} : \mathbb{R}^{N \times p} \times \mathbb{R}^{N \times p} \to \mathbb{R}^{N \times p}$ as

$$\hat{\boldsymbol{u}}_j^{n+1} = \hat{\boldsymbol{u}}_j^n - \frac{\Delta t}{\Delta x} \left(\boldsymbol{G}(\hat{\boldsymbol{u}}_j^n, \hat{\boldsymbol{u}}_{j+1}^n) - \boldsymbol{G}(\hat{\boldsymbol{u}}_{j-1}^n, \hat{\boldsymbol{u}}_j^n) \right) \tag{8}$$

for $j = 1, \cdots, N_x$ and $n = 0, \cdots, N_t$. Here, the number of spatial cells is denoted by N_x and the number of time steps by N_t. The numerical flux is assumed to be consistent, i.e. $\boldsymbol{G}(\hat{\boldsymbol{u}}, \hat{\boldsymbol{u}}) = \boldsymbol{F}(\hat{\boldsymbol{u}})$.

When a consistent numerical flux $\boldsymbol{g} : \mathbb{R}^p \times \mathbb{R}^p \to \mathbb{R}^p$, $\boldsymbol{g} = \boldsymbol{g}(\boldsymbol{u}_\ell, \boldsymbol{u}_r)$ is available for the original problem (1), then for the IPM system we can simply take the numerical flux

$$\tilde{\boldsymbol{G}}(\hat{\boldsymbol{u}}_j^n, \hat{\boldsymbol{u}}_{j+1}^n) = \langle \boldsymbol{g}(\mathcal{U}(\hat{\boldsymbol{u}}_j^n), \mathcal{U}(\hat{\boldsymbol{u}}_{j+1}^n)) \boldsymbol{\varphi}^T \rangle^T$$

in (8). Commonly, this integral cannot be evaluated analytically and therefore needs to be approximated by a quadrature rule

$$\langle h \rangle \approx \langle h \rangle_Q := \sum_{k=1}^{Q} w_k h(\boldsymbol{\xi}_k) f_\Xi(\boldsymbol{\xi}_k).$$

The approximated numerical flux then becomes

$$\boldsymbol{G}(\hat{\boldsymbol{u}}_j^n, \hat{\boldsymbol{u}}_{j+1}^n) = \langle \boldsymbol{g}(\mathcal{U}(\hat{\boldsymbol{u}}_j^n), \mathcal{U}(\hat{\boldsymbol{u}}_{j+1}^n)) \boldsymbol{\varphi}^T \rangle_Q^T. \tag{9}$$

Note that the numerical flux requires evaluating the ansatz $\mathcal{U}(\hat{\boldsymbol{u}}_j^n)$. To simplify notation, we define $\boldsymbol{u}_s : \mathbb{R}^s \to \mathbb{R}^s$,

$$\boldsymbol{u}_s(\boldsymbol{\Lambda}) := \left(\nabla_{\boldsymbol{u}} s\right)^{-1}(\boldsymbol{\Lambda}),$$

meaning that the IPM ansatz (7) at cell j in timestep n can be written as

$$\mathcal{U}(\hat{\boldsymbol{u}}_j^n) = \boldsymbol{u}_s(\hat{\boldsymbol{\lambda}}(\hat{\boldsymbol{u}}_j^n)^T \boldsymbol{\varphi}).$$

The computation of the dual variables $\hat{\boldsymbol{\lambda}}_j^n := \hat{\boldsymbol{\lambda}}(\hat{\boldsymbol{u}}_j^n)$ requires solving the dual problem (6) for the moment vector $\hat{\boldsymbol{u}}_j^n$. Hence, to determine the dual variables for a given moment vector $\hat{\boldsymbol{u}}$, the cost function

$$L(\boldsymbol{\lambda}; \hat{\boldsymbol{u}}) := \langle s_*(\boldsymbol{\lambda}^T \boldsymbol{\varphi}) \rangle_Q - \sum_{i \le M} \boldsymbol{\lambda}_i^T \hat{\boldsymbol{u}}_i \tag{10}$$

needs to be minimized. Hence, one needs to find the root of

$$\nabla_{\boldsymbol{\lambda_i}} L(\boldsymbol{\lambda}; \hat{\boldsymbol{u}}) = \langle \nabla s_*(\boldsymbol{\lambda}^T \boldsymbol{\varphi}) \boldsymbol{\varphi}^T \rangle_Q^T - \hat{\boldsymbol{u}}_i = \langle \boldsymbol{u}_s(\boldsymbol{\lambda}^T \boldsymbol{\varphi}) \boldsymbol{\varphi}^T \rangle_Q^T - \hat{\boldsymbol{u}}_i,$$

where we used $\nabla s_* \equiv \boldsymbol{u}_s$. The root is usually determined by using Newton's method. For simplicity, let us define the full gradient of the Lagrangian to be $\nabla_{\boldsymbol{\lambda}} L(\boldsymbol{\lambda}; \hat{\boldsymbol{u}}) \in \mathbb{R}^{N \cdot p}$, i.e. we store all entries in a vector. Newton's method uses the iteration function $\boldsymbol{d} : \mathbb{R}^{N \times p} \times \mathbb{R}^{N \times p} \to \mathbb{R}^{N \times p}$,

$$\boldsymbol{d}(\boldsymbol{\lambda}, \hat{\boldsymbol{u}}) := \boldsymbol{\lambda} - \boldsymbol{H}(\boldsymbol{\lambda})^{-1} \cdot \nabla_{\boldsymbol{\lambda}} L(\boldsymbol{\lambda}; \hat{\boldsymbol{u}}), \tag{11}$$

where $\boldsymbol{H} \in \mathbb{R}^{p \cdot N \times p \cdot N}$ is the Hessian of (10), given by

$$\boldsymbol{H}(\boldsymbol{\lambda}) := \langle \nabla \boldsymbol{u_s}(\boldsymbol{\lambda}^T \boldsymbol{\varphi}) \otimes \boldsymbol{\varphi} \boldsymbol{\varphi}^T \rangle_Q^T.$$

The function $\boldsymbol{d}$ will in the following be called dual iteration function. Now, the Newton iteration for spatial cell j is given by

$$\boldsymbol{\lambda}_j^{(m+1)} = \boldsymbol{d}(\boldsymbol{\lambda}_j^{(m)}, \hat{\boldsymbol{u}}_{\boldsymbol{j}}). \tag{12}$$

The exact dual state is then obtained by computing the fixed point of $\boldsymbol{d}$, meaning that one converges the iteration (12), i.e. $\hat{\boldsymbol{\lambda}}_j^n := \hat{\boldsymbol{\lambda}}(\hat{\boldsymbol{u}}_{\boldsymbol{j}}^{\boldsymbol{n}}) = \lim_{m \to \infty} \boldsymbol{d}(\boldsymbol{\lambda}_j^{(m)}, \hat{\boldsymbol{u}}_{\boldsymbol{j}}^{\boldsymbol{n}})$. To obtain a finite number of iterations for the iteration in cell j, a stopping criterion

$$\sum_{i=0}^{p} \left\| \nabla_{\boldsymbol{\lambda_i}} L(\boldsymbol{\lambda}_j^{(m)}; \hat{\boldsymbol{u}}_j^n) \right\| < \tau \tag{13}$$

is used.

We now write down the entire scheme: To obtain a more compact notation, we define

$$\boldsymbol{c}(\boldsymbol{\lambda}_\ell, \boldsymbol{\lambda}_c, \boldsymbol{\lambda}_r) := \langle \boldsymbol{u}_s(\boldsymbol{\lambda}_c^T \boldsymbol{\varphi}) \boldsymbol{\varphi}^T \rangle_Q^T - \frac{\Delta t}{\Delta x} \left(\langle \boldsymbol{g}(\boldsymbol{u}_s(\boldsymbol{\lambda}_c^T \boldsymbol{\varphi}), \boldsymbol{u}_s(\boldsymbol{\lambda}_r^T \boldsymbol{\varphi})) \boldsymbol{\varphi}^T \rangle_Q^T - \langle \boldsymbol{g}(\boldsymbol{u}_s(\boldsymbol{\lambda}_\ell^T \boldsymbol{\varphi}), \boldsymbol{u}_s(\boldsymbol{\lambda}_c^T \boldsymbol{\varphi})) \boldsymbol{\varphi}^T \rangle_Q^T \right). \tag{14}$$

The moment iteration is then given by

$$\hat{\boldsymbol{u}}_j^{n+1} = \boldsymbol{c}\left(\hat{\boldsymbol{\lambda}}(\hat{\boldsymbol{u}}_{j-1}^n), \hat{\boldsymbol{\lambda}}(\hat{\boldsymbol{u}}_j^n), \hat{\boldsymbol{\lambda}}(\hat{\boldsymbol{u}}_{j+1}^n)\right), \tag{15}$$

where the map from the moment vector to the dual variables, i.e. $\boldsymbol{\lambda}(\hat{\boldsymbol{u}}_j^n)$, is obtained by iterating

$$\boldsymbol{\lambda}_j^{(m+1)} = \boldsymbol{d}(\boldsymbol{\lambda}_j^{(m)}; \hat{\boldsymbol{u}}_j^n). \tag{16}$$

until condition (13) is fulfilled. This gives Algorithm 1.

Algorithm 1 IPM algorithm

for $j = 0$ to $N_x + 1$ **do**
  $\boldsymbol{u}_j^0 \leftarrow \frac{1}{\Delta x}\int_{x_{j-1/2}}^{x_{j+1/2}} \langle u_{\mathrm{IC}}(x,\cdot)\boldsymbol{\varphi}\rangle_Q dx$
for $n = 0$ to N_t **do**
  for $j = 0$ to $N_x + 1$ **do**
    $\boldsymbol{\lambda}_j^{(0)} \leftarrow \hat{\boldsymbol{\lambda}}_j^n$
    while (13) is violated **do**
      $\boldsymbol{\lambda}_j^{(m+1)} \leftarrow \boldsymbol{d}(\boldsymbol{\lambda}_j^{(m)}; \hat{\boldsymbol{u}}_j^n)$
      $m \leftarrow m + 1$
    $\hat{\boldsymbol{\lambda}}_j^{n+1} \leftarrow \boldsymbol{\lambda}_j^{(m)}$
  for $j = 1$ to N_x **do**
    $\hat{\boldsymbol{u}}_j^{n+1} \leftarrow \boldsymbol{c}(\hat{\boldsymbol{\lambda}}_{j-1}^{n+1}, \hat{\boldsymbol{\lambda}}_j^{n+1}, \hat{\boldsymbol{\lambda}}_{j+1}^{n+1})$

3.2. Properties of the kinetic flux

A straight-forward implementation is ensured by the choice of the numerical flux (9). This choice of the numerical flux is common in the field of transport theory, where it is called the *kinetic flux*. By simply taking moments of a given numerical flux for the deterministic problem, the method can easily be applied to various physical problems whenever an implementation of $\boldsymbol{g} = \boldsymbol{g}(\boldsymbol{u}_\ell, \boldsymbol{u}_r)$ is available. Therefore, we call the proposed numerical method *semi-intrusive*.

Intrusive numerical methods which compute arising integrals analytically and therefore directly depend on the moments (i.e. they do not necessitate the evaluation of the gPC expansion on quadrature points) can be constructed by performing a gPC expansion on the system flux directly [24]. Examples can be found in [25, 26, 27]. While the analytic computation of arising integrals is not always more efficient [28, Section 6], it can also complicate recycling a deterministic solver. See Appendix A for a comparison of numerical costs when using Burgers' equation. However, when not using a quadratic entropy in the IPM method or when the physical flux of the deterministic problem is not a polynomial, it is not clear how many quadrature points the numerical quadrature rule requires to guarantee a sufficiently small quadrature error. We will study the approximation properties of IPM with different quadrature orders in Section 7.1.

4. Strategies for steady problems

In the following, we look at steady state problems, i.e. we have

$$\nabla \cdot \boldsymbol{f}(\boldsymbol{u}(\boldsymbol{x}, \boldsymbol{\xi})) = \boldsymbol{0} \quad \text{in } D \tag{17}$$

with adequate boundary conditions. A general strategy for computing the steady state solution to (17) is to introduce a pseudo-time and numerically treat (17) as an unsteady problem. A steady state solution is then obtained by iterating in pseudo-time until the solution remains constant. It is important to point out that the time it takes to converge to a steady state solution is crucially affected by the chosen initial condition

and its distance to the steady state solution. Similar to the unsteady case (1), we can again derive a moment system for (17) given by

$$\nabla \cdot \langle \boldsymbol{f}(\boldsymbol{u}(\boldsymbol{x}, \boldsymbol{\xi}))\boldsymbol{\varphi}^T \rangle^T = \boldsymbol{0} \quad \text{in } D \tag{18}$$

which is again needed for the construction of intrusive methods. By adding a pseudo-time and using the IPM closure, we obtain the same system as in (4), i.e. Algorithm 1 can be used to iterate to a steady state solution. Note that now, the time iteration is not performed for a fixed number of time steps N_t, but until the condition

$$\sum_{j=1}^{N_x} \Delta x_j \|\hat{\boldsymbol{u}}_j^n - \hat{\boldsymbol{u}}_j^{n-1}\| \leq \varepsilon \tag{19}$$

is fulfilled. Since one is generally interested in low order moments such as the expectation value, this residual can be modified by only accounting for the zero order moments.

4.1. Collocation accelerated IPM

Commonly, a great amount of iterations in pseudo-time is needed to converge to a steady state solution. Consequently, the IPM method which requires solving the dual problem (6) in every spatial cell in each iteration becomes prohibitively expensive. We tackle this problem by using IPM only as a postprocesssing step for the steady solution obtained by a cheap method. (Or vice-versa, we use a cheap method as a preprocessing step for IPM). In our case, we perform the preprocessing step with stochastic-Collocation, i.e. we converge the moments to a steady state solution by applying collocation steps. The obtained moments are then used as initial condition for the IPM moment system (for which the moments are no longer a steady state solution). After applying a significantly reduced number of IPM iterations, we obtain a steady state IPM solution. In our numerical experiments presented in section 7, we can show that the overall costs are dominated by the large number of cheap collocation steps and not by the small number of expensive IPM steps, while the solution shows the expected desirable properties of the IPM solution.

Different variants of this method are possible:

- Since the IPM iterations will again modify the steady state Collocation solution, it is not necessary to converge Collocation to the exact steady state solution before starting IPM. Here, one needs to determine an indicator to choose at which residual the collocation iteration is sufficiently accurate and can therefore be switched to IPM.
- The main idea is to use a cheap but inexact method as a preconditioner for an expensive but accurate method. Here, one is not limited in choosing SC and IPM, but one can for example choose Monte Carlo methods as an accelerator or SC with an increased number of quadrature points as the expensive method. Note that in the latter case, a map from the moments to the solution at the increased quadrature set is required, for which the IPM reconstruction (7) would be a suitable choice.

4.2. One-shot IPM

In this section we aim at breaking up the inner loop in the IPM algorithm 1, i.e. to just perform one iteration of the dual problem in each time step. Consequently, the IPM reconstruction given by (5) is not done exactly, meaning that the reconstructed solution does not minimize the entropy while not fulfilling the moment constraint. However, the fact that the moment vectors are not yet converged to the steady solution seems to permit such an inexact reconstruction. Hence, we aim at iterating the moments to steady state and the dual variables to the exact solution of the IPM optimization problem (5) simultaneously. By successively performing one update of the moment iteration and one update of the dual iteration, we obtain

$$\boldsymbol{\lambda}_j^{n+1} = \boldsymbol{d}(\boldsymbol{\lambda}_j^n, \boldsymbol{u}_j^n) \quad \text{for all j} \tag{20a}$$

$$\boldsymbol{u}_j^{n+1} = \boldsymbol{c}\left(\boldsymbol{\lambda}_{j-1}^{n+1}, \boldsymbol{\lambda}_j^{n+1}, \boldsymbol{\lambda}_{j+1}^{n+1}\right). \tag{20b}$$

This gives algorithm

Algorithm 2 One-shot IPM implementation

for $j = 0$ to $N_x + 1$ **do**
    $\boldsymbol{u}_j^0 \leftarrow \frac{1}{\Delta x} \int_{x_{j-1/2}}^{x_{j+1/2}} \langle u_{\mathrm{IC}}(x, \cdot)\boldsymbol{\varphi} \rangle_Q dx$
while (19) is violated **do**
    for $j = 1$ to N_x **do**
        $\boldsymbol{\lambda}_j^{n+1} \leftarrow \boldsymbol{d}(\boldsymbol{\lambda}_j^n; \hat{\boldsymbol{u}}_j^n)$
        $\hat{\boldsymbol{u}}_j^{n+1} \leftarrow \boldsymbol{c}(\boldsymbol{\lambda}_{j-1}^{n+1}, \boldsymbol{\lambda}_j^{n+1}, \boldsymbol{\lambda}_{j+1}^{n+1})$
    $n \leftarrow n + 1$

We call this method One-Shot IPM, since it is inspired by One-shot optimization, see for example [23], which uses only a single iteration of the primal and dual step in order to update the design variables. Note that the dual variables from the One-Shot iteration are written without a hat to indicate that they are not the exact solution of the dual problem.

In the following, we will show that this iteration converges, if the chosen initial condition is sufficiently close to the steady state solution. For this we take an approach commonly chosen to prove local convergence properties of Newton's method: In Theorem 1, we show that the iteration function is contractive at its fixed point and conclude in Theorem 2 that this yields local convergence:

Theorem 1. *Assume that the classical IPM iteration is contractive at its fixed point $\hat{\boldsymbol{u}}^*$. Then the Jacobi matrix $\boldsymbol{J}$ of the One-Shot IPM iteration* (20) *has a spectral radius $\rho(\boldsymbol{J}) < 1$ at the fixed point $(\boldsymbol{\lambda}^*, \hat{\boldsymbol{u}}^*)$.*

Proof. First, to understand what contraction of the classical IPM iteration implies, we rewrite the moment iteration (15) of the classical IPM scheme: When defining the update function

$$\tilde{\boldsymbol{c}}\left(\hat{\boldsymbol{u}}_\ell, \hat{\boldsymbol{u}}_c, \hat{\boldsymbol{u}}_r\right) := \boldsymbol{c}\left(\hat{\boldsymbol{\lambda}}(\hat{\boldsymbol{u}}_\ell), \hat{\boldsymbol{\lambda}}(\hat{\boldsymbol{u}}_c), \hat{\boldsymbol{\lambda}}(\hat{\boldsymbol{u}}_r)\right)$$

we can rewrite the classical moment iteration as

$$\hat{\boldsymbol{u}}_j^{n+1} = \tilde{\boldsymbol{c}}\left(\hat{\boldsymbol{u}}_{j-1}^n, \hat{\boldsymbol{u}}_j^n, \hat{\boldsymbol{u}}_{j+1}^n\right). \tag{21}$$

Since we assume that the classical IPM scheme is contractive at its fixed point, we have $\rho(\nabla_{\hat{\boldsymbol{u}}} \tilde{\boldsymbol{c}}(\hat{\boldsymbol{u}}^*)) < 1$ with $\nabla_{\hat{\boldsymbol{u}}} \tilde{\boldsymbol{c}} \in \mathbb{R}^{N \cdot N_x \times N \cdot N_x}$ defined by

$$\nabla_{\hat{\boldsymbol{u}}} \tilde{\boldsymbol{c}} = \begin{pmatrix} \partial_{\hat{\boldsymbol{u}}_c} \tilde{\boldsymbol{c}}_1 & \partial_{\hat{\boldsymbol{u}}_r} \tilde{\boldsymbol{c}}_1 & 0 & 0 & \dots \\ \partial_{\hat{\boldsymbol{u}}_\ell} \tilde{\boldsymbol{c}}_2 & \partial_{\hat{\boldsymbol{u}}_c} \tilde{\boldsymbol{c}}_2 & \partial_{\hat{\boldsymbol{u}}_r} \tilde{\boldsymbol{c}}_2 & 0 & \dots \\ 0 & \partial_{\hat{\boldsymbol{u}}_\ell} \tilde{\boldsymbol{c}}_3 & \partial_{\hat{\boldsymbol{u}}_c} \tilde{\boldsymbol{c}}_3 & \partial_{\hat{\boldsymbol{u}}_r} \tilde{\boldsymbol{c}}_3 & \\ \vdots & & & \ddots & \\ 0 & \cdots & 0 & \partial_{\hat{\boldsymbol{u}}_\ell} \tilde{\boldsymbol{c}}_{N_x} & \partial_{\hat{\boldsymbol{u}}_c} \tilde{\boldsymbol{c}}_{N_x} \end{pmatrix},$$

where we define $\tilde{\boldsymbol{c}}_j := \tilde{\boldsymbol{c}}\left(\hat{\boldsymbol{u}}_{j-1}^*, \hat{\boldsymbol{u}}_j^*, \hat{\boldsymbol{u}}_{j+1}^*\right)$ for all j. Now for each term inside the matrix $\nabla_{\hat{\boldsymbol{u}}} \tilde{\boldsymbol{c}}$ we have

$$\partial_{\hat{\boldsymbol{u}}_\ell} \tilde{\boldsymbol{c}}_j = \frac{\partial \boldsymbol{c}_j}{\partial \hat{\boldsymbol{\lambda}}_\ell} \frac{\partial \hat{\boldsymbol{\lambda}}(\hat{\boldsymbol{u}}_{j-1}^*)}{\partial \hat{\boldsymbol{u}}}, \quad \partial_{\hat{\boldsymbol{u}}_c} \tilde{\boldsymbol{c}}_j = \frac{\partial \boldsymbol{c}_j}{\partial \hat{\boldsymbol{\lambda}}_c} \frac{\partial \hat{\boldsymbol{\lambda}}(\hat{\boldsymbol{u}}_j^*)}{\partial \hat{\boldsymbol{u}}}, \quad \partial_{\hat{\boldsymbol{u}}_r} \tilde{\boldsymbol{c}}_j = \frac{\partial \boldsymbol{c}_j}{\partial \hat{\boldsymbol{\lambda}}_r} \frac{\partial \hat{\boldsymbol{\lambda}}(\hat{\boldsymbol{u}}_{j+1}^*)}{\partial \hat{\boldsymbol{u}}}. \tag{22}$$

We first wish to understand the structure of the terms $\partial_{\hat{\boldsymbol{u}}} \hat{\boldsymbol{\lambda}}(\hat{\boldsymbol{u}})$. For this, we note that the exact dual variables fulfill

$$\hat{\boldsymbol{u}} = \langle \boldsymbol{u}_s(\hat{\boldsymbol{\lambda}}^T \boldsymbol{\varphi}) \boldsymbol{\varphi}^T \rangle =: \boldsymbol{h}(\hat{\boldsymbol{\lambda}}), \tag{23}$$

which is why we have the mapping $\hat{\boldsymbol{u}} : \mathbb{R}^{N\times p} \to \mathbb{R}^{N\times p}$, $\hat{\boldsymbol{u}}(\hat{\boldsymbol{\lambda}}) = \boldsymbol{h}(\hat{\boldsymbol{\lambda}})$. Since the solution of the dual problem for a given moment vector is unique, this mapping is bijective and therefore we have an inverse function

$$\hat{\boldsymbol{\lambda}} = \boldsymbol{h}^{-1}(\hat{\boldsymbol{u}}(\hat{\boldsymbol{\lambda}})). \tag{24}$$

Now we differentiate both sides w.r.t. $\hat{\boldsymbol{\lambda}}$ to get

$$\boldsymbol{I}_d = \frac{\partial \boldsymbol{h}^{-1}(\hat{\boldsymbol{u}}(\hat{\boldsymbol{\lambda}}))}{\partial \hat{\boldsymbol{u}}} \frac{\partial \hat{\boldsymbol{u}}(\hat{\boldsymbol{\lambda}})}{\partial \hat{\boldsymbol{\lambda}}}.$$

We multiply with the matrix inverse of $\frac{\partial \hat{\boldsymbol{u}}(\hat{\boldsymbol{\lambda}})}{\partial \hat{\boldsymbol{\lambda}}}$ to get

$$\left(\frac{\partial \hat{\boldsymbol{u}}(\hat{\boldsymbol{\lambda}})}{\partial \hat{\boldsymbol{\lambda}}}\right)^{-1} = \frac{\partial \boldsymbol{h}^{-1}(\hat{\boldsymbol{u}}(\hat{\boldsymbol{\lambda}}))}{\partial \hat{\boldsymbol{u}}}.$$

Note that on the left-hand-side we have the inverse of a matrix and on the right-hand-side, we have the inverse of a multi-dimensional function. By rewriting $\boldsymbol{h}^{-1}(\hat{\boldsymbol{u}}(\hat{\boldsymbol{\lambda}}))$ as $\hat{\boldsymbol{\lambda}}(\hat{\boldsymbol{u}})$ and simply computing the term $\frac{\partial \hat{\boldsymbol{u}}(\hat{\boldsymbol{\lambda}})}{\partial \hat{\boldsymbol{\lambda}}}$ by differentiating (23) w.r.t. $\hat{\boldsymbol{\lambda}}$, one obtains

$$\partial_{\hat{\boldsymbol{u}}} \hat{\boldsymbol{\lambda}}(\hat{\boldsymbol{u}}) = \langle \nabla \boldsymbol{u}_s(\hat{\boldsymbol{\lambda}}^T \boldsymbol{\varphi}) \boldsymbol{\varphi} \boldsymbol{\varphi}^T \rangle^{-T}. \tag{25}$$

Now we begin to derive the spectrum of the *One-Shot IPM* iteration (20). Note that in its current form this iteration is not really a fixed point iteration, since it uses the time updated dual variables in (20b). To obtain a fixed point iteration, we plug the dual iteration step (20a) into the moment iteration (20b) to obtain

$$\begin{aligned}
\boldsymbol{\lambda}_j^{n+1} &= \boldsymbol{d}(\boldsymbol{\lambda}_j^n, \hat{\boldsymbol{u}}_j^n) \quad \text{for all j} \\
\hat{\boldsymbol{u}}_j^{n+1} &= \boldsymbol{c}\left(\boldsymbol{d}(\boldsymbol{\lambda}_{j-1}^n, \hat{\boldsymbol{u}}_{j-1}^n), \boldsymbol{d}(\boldsymbol{\lambda}_j^n, \hat{\boldsymbol{u}}_j^n), \boldsymbol{d}(\boldsymbol{\lambda}_{j+1}^n, \hat{\boldsymbol{u}}_{j+1}^n)\right)
\end{aligned}$$

The Jacobian $\boldsymbol{J} \in \mathbb{R}^{2N\cdot N_x \times 2N \cdot N_x}$ has the form

$$\boldsymbol{J} = \begin{pmatrix} \partial_{\boldsymbol{\lambda}} \boldsymbol{d} & \partial_{\hat{\boldsymbol{u}}} \boldsymbol{d} \\ \partial_{\boldsymbol{\lambda}} \boldsymbol{c} & \partial_{\hat{\boldsymbol{u}}} \boldsymbol{c} \end{pmatrix}, \tag{26}$$

where each block has entries for all spatial cells. We start by looking at $\partial_{\boldsymbol{\lambda}} \boldsymbol{d}$. For the columns belonging to cell j, we have

$$\begin{aligned}
\partial_{\boldsymbol{\lambda}} \boldsymbol{d}(\boldsymbol{\lambda}_j^n, \hat{\boldsymbol{u}}_j^n) &= \boldsymbol{I}_d - \boldsymbol{H}(\boldsymbol{\lambda})^{-1} \cdot \langle \nabla \boldsymbol{u}_s(\boldsymbol{\varphi}^T \boldsymbol{\lambda}_j^n) \boldsymbol{\varphi} \boldsymbol{\varphi}^T \rangle^T - \partial_{\boldsymbol{\lambda}} \boldsymbol{H}(\boldsymbol{\lambda})^{-1} \cdot \left(\langle \boldsymbol{u}_s(\boldsymbol{\varphi}^T \boldsymbol{\lambda}_j^n) \boldsymbol{\varphi}^T \rangle^T - \hat{\boldsymbol{u}} \right) \\
&= -\partial_{\boldsymbol{\lambda}} \boldsymbol{H}(\boldsymbol{\lambda})^{-1} \cdot \left(\langle \boldsymbol{u}_s(\boldsymbol{\varphi}^T \boldsymbol{\lambda}_j^n) \boldsymbol{\varphi}^T \rangle^T - \hat{\boldsymbol{u}} \right).
\end{aligned}$$

Recall that at the fixed point $(\boldsymbol{\lambda}^*, \hat{\boldsymbol{u}}^*)$, we have $\langle \boldsymbol{u}_s(\boldsymbol{\varphi}^T \boldsymbol{\lambda}_j^n) \boldsymbol{\varphi}^T \rangle^T = \hat{\boldsymbol{u}}$, hence one obtains $\partial_{\boldsymbol{\lambda}} \boldsymbol{d} = \boldsymbol{0}$. For the block $\partial_{\hat{\boldsymbol{u}}} \boldsymbol{d}$, we get

$$\partial_{\hat{\boldsymbol{u}}} \boldsymbol{d}(\boldsymbol{\lambda}_j^n, \hat{\boldsymbol{u}}_j^n) = \boldsymbol{H}(\boldsymbol{\lambda})^{-1},$$

hence $\partial_{\hat{\boldsymbol{u}}} \boldsymbol{d}$ is a block diagonal matrix. Let us now look at $\partial_{\boldsymbol{\lambda}} \boldsymbol{c}$ at a fixed spatial cell j:

$$\frac{\partial \boldsymbol{c}}{\partial \boldsymbol{\lambda}_\ell} \frac{\partial \boldsymbol{d}(\boldsymbol{\lambda}_{j-1}^n, \hat{\boldsymbol{u}}_{j-1}^n)}{\partial \boldsymbol{\lambda}} = \boldsymbol{0},$$

since we already showed that by the choice of $\boldsymbol{H}(\boldsymbol{\lambda})^{-1}$ the term $\partial_{\boldsymbol{\lambda}} \boldsymbol{d}$ is zero. We can show the same result for all spatial cells and all inputs of $\boldsymbol{c}$ analogously, hence $\partial_{\boldsymbol{\lambda}} \boldsymbol{c} = \boldsymbol{0}$. For the last block, we have that

$$\frac{\partial \boldsymbol{c}}{\partial \boldsymbol{\lambda}_\ell} \frac{\partial \boldsymbol{d}(\boldsymbol{\lambda}_{j-1}^n, \hat{\boldsymbol{u}}_{j-1}^n)}{\partial \hat{\boldsymbol{u}}} = \frac{\partial \boldsymbol{c}}{\partial \boldsymbol{\lambda}_\ell} \boldsymbol{H}(\boldsymbol{\lambda})^{-1} = \frac{\partial \boldsymbol{c}}{\partial \boldsymbol{\lambda}_\ell} \langle \nabla \boldsymbol{u}_s(\boldsymbol{\varphi}^T \boldsymbol{\lambda}_{j-1}^n) \boldsymbol{\varphi} \boldsymbol{\varphi}^T \rangle^{-T} = \partial_{\hat{\boldsymbol{u}}_\ell} \tilde{\boldsymbol{c}}_j$$

by the choice of $\boldsymbol{H}(\boldsymbol{\lambda})^{-1}$ as well as (22) and (25). We obtain an analogous result for the second and third input. Hence, we have that $\partial_{\hat{\boldsymbol{u}}}\boldsymbol{c} = \nabla_{\hat{\boldsymbol{u}}}\tilde{\boldsymbol{c}}$, which only has eigenvalues between -1 and 1 by the assumption that the classical IPM iteration is contractive. Since $\boldsymbol{J}$ is an upper triangluar block matrix, the eigenvalues are given by $\lambda\left(\partial_{\boldsymbol{\lambda}}\boldsymbol{d}\right) = 0$ and $\lambda\left(\partial_{\hat{\boldsymbol{u}}}\boldsymbol{c}\right) \in (-1, 1)$, hence the One-Shot IPM is contractive around its fixed point. □

Theorem 2. *With the assumptions from Theorem 1, the One-Shot IPM converges locally, i.e. there exists a $\delta > 0$ s.t. for all starting points $(\boldsymbol{\lambda}^0, \hat{\boldsymbol{u}}^0) \in B_\delta(\boldsymbol{\lambda}^*, \hat{\boldsymbol{u}}^*)$ we have*

$$\|(\boldsymbol{\lambda}^n, \hat{\boldsymbol{u}}^n) - (\boldsymbol{\lambda}^*, \hat{\boldsymbol{u}}^*)\| \to 0 \qquad \text{for } n \to \infty.$$

Proof. By Theorem 1, the One-Shot scheme is contractive at its fixed point. Since we assumed convergence of the classical IPM scheme, we can conclude that all entries in the Jacobian $\boldsymbol{J}$ are continuous functions. Furthermore, the determinant of $\tilde{\boldsymbol{J}} := \boldsymbol{J} - \lambda \boldsymbol{I}_d$ is a polynomial of continuous functions, since

$$\det(\tilde{\boldsymbol{J}}) = \sum_{\sigma} \operatorname{sgn}(\sigma) \prod_{i=1}^{2N_x N} \tilde{J}_{\sigma(i),i}.$$

Since the roots of a polynomial vary continuously with its coefficients, the eigenvalues of $\boldsymbol{J}$ are continuous w.r.t $(\boldsymbol{\lambda}, \hat{\boldsymbol{u}})$. Hence there exists an open ball with radius δ around the fixed point in which the eigenvalues remain in the interval $(-1, 1)$. □

Remark 3. *Since the preconditioning step of the Collocation-accelerated IPM method generates initial conditions which are close to the steady state solution, using One-Shot IPM instead of classical IPM is well suited. However, our numerical calculations show that one-shot IPM converges even if the solution is far away from its steady state.*

5. Adaptivity

The following section presents the adaptivity strategy used in this work. Since stochastic hyperbolic problems generally experience shocks in a small portion of the space-time domain, the idea is to perform arising computations on a high accuracy level in this small area, while keeping a low level of accuracy in the remainder. The hope is to achieve the finest level accuracy with this adaptive strategy, i.e. the same error is obtained while using a significantly reduced number of unknowns.

In the following, we discuss the building blocks of the IPM method for accuracy levels $\ell = 1, \cdots, N_{\text{ad}}$. At a given level ℓ, the total degree of the basis function is given by M_ℓ with a corresponding number of moments N_ℓ. The number of quadrature points at level ℓ is denoted by Q_ℓ. To determine the accuracy level of a given moment vector $\hat{\boldsymbol{u}}$ we choose techniques used in discontinuous Galerkin (DG) methods. Adaptivity is a common strategy to accelerate this class of methods and several indicators to determine the smoothness of the solution exist. We make use of a strategy from [29], which uses the highest degree moments as indicator. Translating the idea of the discontinuity sensor used in [29] to uncertainty quantification, we define the polynomial approximation at level ℓ as

$$\tilde{\boldsymbol{u}}_\ell := \sum_{|i| \le M_\ell} \hat{\boldsymbol{u}}_i \varphi_i.$$

Now the indicator for a moment vector at level ℓ is defined as

$$\boldsymbol{S}_\ell := \frac{\langle (\tilde{\boldsymbol{u}}_\ell - \tilde{\boldsymbol{u}}_{\ell-1})^2 \rangle}{\langle \tilde{\boldsymbol{u}}_\ell^2 \rangle}, \tag{27}$$

where divisions and multiplications are performed element-wise. Note that a similar indicator has been used in [19] for intrusive methods in uncertainty quantification. In this work, we use the first entry in $\boldsymbol{S}_\ell$ to

determine the refinement level, i.e. in the case of gas dynamics, the regularity of the density is chosen to indicate an adequate refinement level. If the moment vector in a given cell at a certain timestep is initially at refinement level ℓ, this level is kept if the error indicator (27) lies in the interval $I_\delta := [\delta_-, \delta_+]$. Here $\delta_\pm$ are user determined parameters. If the indicator is smaller than δ_-, the refinement level is decreased, if it lies above δ_+, it is increased.

Now we need to specify how the different building blocks of IPM can be modified to work with varying truncation orders in different cells. Let us first add dimensions to the notation of the dual iteration function $\boldsymbol{d}$, which has been defined in (11). Now, we have $\boldsymbol{d}_\ell : \mathbb{R}^{N_\ell \times p} \times \mathbb{R}^{N_\ell \times p} \to \mathbb{R}^{N_\ell \times p}$, given by

$$\boldsymbol{d}_\ell(\boldsymbol{\lambda}, \hat{\boldsymbol{u}}) := \boldsymbol{\lambda} - \boldsymbol{H}_\ell^{-1}(\boldsymbol{\lambda}) \cdot \left(\langle \boldsymbol{u}_s(\boldsymbol{\lambda}^T \boldsymbol{\varphi}_\ell) \boldsymbol{\varphi}_\ell^T \rangle_{Q_\ell}^T - \hat{\boldsymbol{u}} \right), \tag{28}$$

where $\boldsymbol{\varphi}_\ell \in \mathbb{R}^{N_\ell}$ collects all basis functions with total degree smaller or equal to M_ℓ. The Hessian $\boldsymbol{H}_\ell$ is given by

$$\boldsymbol{H}_\ell(\boldsymbol{\lambda}) := \langle \nabla \boldsymbol{u}_{\boldsymbol{s}}(\boldsymbol{\lambda}^T \boldsymbol{\varphi}_\ell) \otimes \boldsymbol{\varphi}_\ell \boldsymbol{\varphi}_\ell^T \rangle_{Q_\ell}^T.$$

An adaptive version of the moment iteration (14) is denoted by $\boldsymbol{c}_\ell^{\boldsymbol{\ell}'} : \mathbb{R}^{N_{\ell_1'} \times p} \times \mathbb{R}^{N_{\ell_2'} \times p} \times \mathbb{R}^{N_{\ell_3'} \times p} \to \mathbb{R}^{N_\ell \times p}$ and given by

$$\boldsymbol{c}_\ell^{\boldsymbol{\ell}'}(\boldsymbol{\lambda}_1, \boldsymbol{\lambda}_2, \boldsymbol{\lambda}_3) := \langle \boldsymbol{u}_s(\boldsymbol{\lambda}_2^T \boldsymbol{\varphi}_{\ell_2'}) \boldsymbol{\varphi}_\ell^T \rangle_{Q_\ell}^T - \frac{\Delta t}{\Delta x} \left(\langle \boldsymbol{g}(\boldsymbol{u}_s(\boldsymbol{\lambda}_2^T \boldsymbol{\varphi}_{\ell_2'}), \boldsymbol{u}_s(\boldsymbol{\lambda}_3^T \boldsymbol{\varphi}_{\ell_3'})) \boldsymbol{\varphi}_\ell^T \rangle_{Q_\ell}^T - \langle \boldsymbol{g}(\boldsymbol{u}_s(\boldsymbol{\lambda}_1^T \boldsymbol{\varphi}_{\ell_1'}), \boldsymbol{u}_s(\boldsymbol{\lambda}_2^T \boldsymbol{\varphi}_{\ell_2'})) \boldsymbol{\varphi}_\ell^T \rangle_{Q_\ell}^T \right). \tag{29}$$

Hence, the index vector $\boldsymbol{\ell}' \in \mathbb{N}^3$ denotes the refinement levels of the stencil cells, which are used to compute the time updated moment vector at level ℓ.

The strategy now is to perform the dual update for a set of moment vectors $\hat{\boldsymbol{u}}_j^n$ at refinement levels ℓ_j^n for $j = 1, \cdots, N_x$. Hence, the dual iteration makes use of the iteration function (28) at refinement level ℓ_j^n. After that, the refinement level at the next time step ℓ_j^{n+1} is determined by making use of the smoothness indicator (27). The moment update then computes the moments at the time updated refinement level ℓ_j^{n+1} making use of the dual states at the old refinement levels $\boldsymbol{\ell}' = (\ell_{j-1}^n, \ell_j^n, \ell_{j+1}^n)^T$. The IPM algorithm with adaptivity then reads

Algorithm 3 Adaptive IPM implementation

for $j = 0$ to $N_x + 1$ **do**
  $\ell_j^0 \leftarrow$ choose initial refinement level
  $\boldsymbol{u}_j^0 \leftarrow \frac{1}{\Delta x} \int_{x_{j-1/2}}^{x_{j+1/2}} \langle u_{\mathrm{IC}}(x, \cdot) \boldsymbol{\varphi}_{\ell_j^0} \rangle_{Q_{\ell_j^0}} dx$
for $n = 0$ to N_t **do**
  for $j = 0$ to $N_x + 1$ **do**
    $\boldsymbol{\lambda}_j^{(0)} \leftarrow \hat{\boldsymbol{\lambda}}_j^n$
    while (13) is violated **do**
      $\boldsymbol{\lambda}_j^{(m+1)} \leftarrow \boldsymbol{d}_{\ell_j^n}(\boldsymbol{\lambda}_j^{(m)}; \hat{\boldsymbol{u}}_j^n)$
      $m \leftarrow m + 1$
    $\hat{\boldsymbol{\lambda}}_j^{n+1} \leftarrow \boldsymbol{\lambda}_j^{(m)}$
    $\ell_j^{n+1} \leftarrow$ DetermineRefinementLevel $\left(\hat{\boldsymbol{\lambda}}_j^{n+1} \right)$
  for $j = 1$ to N_x **do**
    $\boldsymbol{\ell}' \leftarrow (\ell_{j-1}^n, \ell_j^n, \ell_{j+1}^n)^T$
    $\hat{\boldsymbol{u}}_j^{n+1} \leftarrow \boldsymbol{c}_{\ell_j^{n+1}}^{\boldsymbol{\ell}'}(\hat{\boldsymbol{\lambda}}_{j-1}^{n+1}, \hat{\boldsymbol{\lambda}}_j^{n+1}, \hat{\boldsymbol{\lambda}}_{j+1}^{n+1})$

Adaptivity can be used for intrusive methods in general as well as for steady and unsteady problems. In the case of steady problems, we can make use of a strategy, which we call *refinement retardation*. Recall that the convergence to an admissible steady state solution is expensive and a high accuracy and desirable solution properties are only required at the end of this iteration process. Hence, we propose to iteratively increase the maximal refinement level whenever a certain residual (19) is fulfilled. For a given set of maximal refinement levels ℓ_m^* and a set of residuals ε_m^* at which the refinement level must be increased we can now perform a large amount of th required iterations on a lower but cheaper accuracy level. The same strategy can be applied for one-shot IPM. In this case, the algorithm is given by

Algorithm 4 Adaptive one-shot IPM implementation with refinement retardation

1: **for** $j = 0$ to $N_x + 1$ **do**
2: $\quad \boldsymbol{u}_j^0 \leftarrow \frac{1}{\Delta x} \int_{x_{j-1/2}}^{x_{j+1/2}} \langle u_{\mathrm{IC}}(x, \cdot) \boldsymbol{\varphi} \rangle_Q dx$
3: **while** (19) is violated **do**
4: $\quad$ **for** $j = 1$ to N_x **do**
5: $\quad\quad \boldsymbol{\lambda}_j^{n+1} \leftarrow \boldsymbol{d}_{\ell_j^n}(\boldsymbol{\lambda}_j^n; \hat{\boldsymbol{u}}_j^n)$
6: $\quad\quad \ell_j^{n+1} \leftarrow \max\{\text{DetermineRefinementLevel}\left(\boldsymbol{\lambda}_j^{n+1}\right), \ell_m^*\}$
7: $\quad\quad \boldsymbol{\ell}' \leftarrow (\ell_{j-1}^n, \ell_j^n, \ell_{j+1}^n)^T$
8: $\quad\quad \hat{\boldsymbol{u}}_j^{n+1} \leftarrow \boldsymbol{c}_{\ell_j^{n+1}}^{\boldsymbol{\ell}'}(\boldsymbol{\lambda}_{j-1}^{n+1}, \boldsymbol{\lambda}_j^{n+1}, \boldsymbol{\lambda}_{j+1}^{n+1})$
9: $\quad n \leftarrow n + 1$
10: $\quad$ **if** (19) fulfills the stopping criterion ε_m^* **then**
11: $\quad\quad m \leftarrow m + 1$

6. Parallelization and Implementation

It remains to discuss the parallelization of the presented algorithms. In order to minimize the parallelization overhead, our goal is to minimize the need to send data between processors. Note that the dual problem (line 8 in Algorithm 3 and line 5 in Algorithm 4) does not have a stencil, i.e. it suffices to distribute the spatial cells between processors. In contrast to that, the finite volume update (line 14 in Algorithm 3 and line 8 in Algorithm 4) has a stencil. Hence, distributing the spatial mesh between processors will yield communication overhead since data needs to be sent whenever a stencil cell lies on a different processor. Therefore, we choose to parallelize the quadrature points, which again minimizes communication effort. As mentioned in Section 3.2, we first compute the solution at stencil cells for all quadrature points. I.e. we determine $\boldsymbol{u}_k^{(j)} \in \mathbb{R}^p$ and the corresponding stencil cells for $k = 1, \cdots, Q$ by

$$\boldsymbol{u}_k^{(j-1)} := \boldsymbol{u}_s(\boldsymbol{\lambda}_{j-1}^T \boldsymbol{\varphi}_{\ell_1'}(\boldsymbol{\xi}_k)), \quad \boldsymbol{u}_k^{(j)} := \boldsymbol{u}_s(\boldsymbol{\lambda}_j^T \boldsymbol{\varphi}_{\ell_2'}(\boldsymbol{\xi}_k)), \quad \boldsymbol{u}_k^{(j+1)} := \boldsymbol{u}_s(\boldsymbol{\lambda}_{j+1}^T \boldsymbol{\varphi}_{\ell_3'}(\boldsymbol{\xi}_k)).$$

Then, the finite volume update function (29) can be written as

$$\boldsymbol{c}_\ell^{\boldsymbol{\ell}'}(\boldsymbol{\lambda}_1, \boldsymbol{\lambda}_2, \boldsymbol{\lambda}_3) = \sum_{k=1}^{Q} w_k \left[\boldsymbol{u}_k^{(j)} - \frac{\Delta t}{\Delta x} \left(\boldsymbol{g}(\boldsymbol{u}_k^{(j)}, \boldsymbol{u}_k^{(j+1)}) - \boldsymbol{g}(\boldsymbol{u}_k^{(j-1)}, \boldsymbol{u}_k^{(j)}) \right) \right] \boldsymbol{\varphi}_\ell(\boldsymbol{\xi}_k)^T. \tag{30}$$

Instead of distributing the mesh on the different processors, we now distribute the quadrature set, i.e. the sum in (30) can be computed in parallel. Now after having performed the dual update, the dual variables are send to all processors. With these variables, each processor computes the solution on its portion of the quadrature set and then computed its part of the sum in (30) on all spacial cells. All parts from the different processors are then added together and the full time-updated moments are distributed to all processors. From here, the dual update can again be performed. The standard IPM Algorithm 1 and one-shot IPM 2 use this parallelization strategy accordingly. Again, we point out that stochastic-Galerkin is a variant of IPM, i.e. all presented techniques for IPM can also be used for SG. The SC algorithm that we use

to compare intrusive with non-intrusive methods uses a given deterministic solver as a black box. Here, we distribute the quadrature set between all processors. Note that both, SC and IPM are based on the same deterministic solver, i.e. we use the same deterministic numerical flux $\boldsymbol{g}$. This allows a fair comparison of the different intrusive and non-intrusive techniques.

7. Results

7.1. 2D Euler equations with a one dimensional uncertainty

We start by quantifying the effects of an uncertain angle of attack $\phi \sim U(0.75, 1.75)$ for a NACA0012 airfoil computed with different methods. The stochastic Euler equations in two dimensions are given by

$$\partial_t \begin{pmatrix} \rho \\ \rho v_1 \\ \rho v_2 \\ \rho e \end{pmatrix} + \partial_{x_1} \begin{pmatrix} \rho v_1 \\ \rho v_1^2 + p \\ \rho v_1 v_2 \\ v_1(\rho e + p) \end{pmatrix} + \partial_{x_2} \begin{pmatrix} \rho v_2 \\ \rho v_1 v_2 \\ \rho v_2^2 + p \\ v_2(\rho e + p) \end{pmatrix} = \mathbf{0}.$$

These equations determine the time evolution of the conserved variables $(\rho, \rho \boldsymbol{v}, \rho e)$, i.e. density, momentum and energy. A closure for the pressure p is given by

$$p = (\gamma - 1)\rho \left(e - \frac{1}{2}(v_1^2 + v_2^2) \right).$$

Since the fluid of the following test cases is air, we choose the heat capacity ratio γ to be 1.4. The spatial mesh discretizes the flow domain around the airfoil. At the airfoil boundary Γ_0, we use the Euler slip condition $\boldsymbol{v}^T \boldsymbol{n} = 0$, where $\boldsymbol{n}$ denotes the surface normal. At a sufficiently large distance away from the airfoil, we assume a far field flow with a given Mach number $Ma = 0.8$, pressure $p = 101\,325$ Pa and a temperature of 273.15 K. Now the angle of attack ϕ is uniformly distributed in the interval of $[0.75, 1.75]$ degrees. I.e. we choose $\phi(\xi) = 1.25 + 0.5\xi$ where $\xi \sim U(-1, 1)$. As commonly done, the initial condition is equal to the far field boundary values. Consequently, the wall condition at the airfoil is violated and will correct the flow solution.

The computational domain is a circle with a diameter of 40 meters. In the center, the NACA0012 airfoil with a length of one meter is located. The discretization is composed of a coarsely refined far field and a finely resolved region around the airfoil, since we are interested in the flow solution at the airfoil. Altogether, the mesh consists of 22361 triangular elements.

The aim is to quantify the effects arising from the one-dimensional uncertainty ξ and to investigate its effects on the solution with different methods. To be able to measure the quality of the obtained solutions, we compute a reference solution using stochastic-Collocation with 100 Gauss-Lobatto quadrature points, which can be found in Figure 1. In the following, we investigate the L^2 error of the variance and the expectation value. The L^2 error of the discrete quantity $\boldsymbol{e}_\Delta = (\boldsymbol{e}_1, \cdots, \boldsymbol{e}_{N_x})^T$, where $\boldsymbol{e}_j$ denotes the cell average in spatial cell j is denoted by

$$\|\boldsymbol{e}_\Delta\|_\Delta := \sqrt{\sum_{j=1}^{N_x} \Delta x_j \boldsymbol{e}_j^2}.$$

Hence, when denoting the reference solution by $\boldsymbol{u}_\Delta$ and the moments obtained with the numerical method by $\hat{\boldsymbol{u}}_\Delta$, we investigate the relative error

$$\frac{\|E[\boldsymbol{u}_\Delta] - E[\mathcal{U}(\hat{\boldsymbol{u}}_\Delta)]\|_\Delta}{\|E[\mathcal{U}(\hat{\boldsymbol{u}}_\Delta)]\|_\Delta} \qquad \text{and} \qquad \frac{\|Var[\boldsymbol{u}_\Delta] - Var[\mathcal{U}(\hat{\boldsymbol{u}}_\Delta)]\|_\Delta}{\|Var[\mathcal{U}(\hat{\boldsymbol{u}}_\Delta)]\|_\Delta}.$$

The error is computed inside a box of one meter height and 1.1 meters length around the airfoil to prevent small fluctuations in the coarsely refined far field from affecting the error.

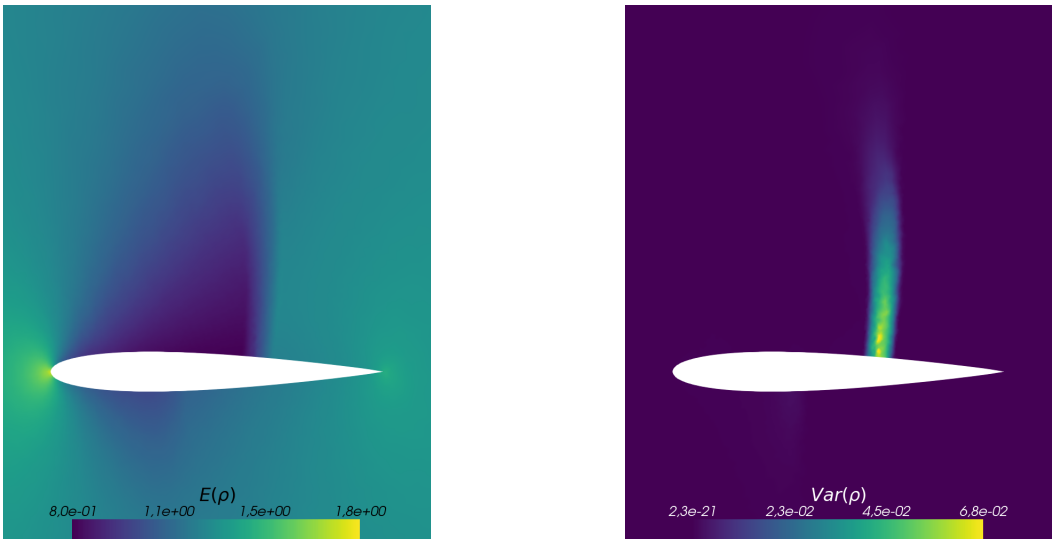

Figure 1: Reference solution E[ρ] and Var[ρ].

The quantities of interests are now computed with the different methods. All methods in this section have been computed using five MPI threads. For more information on the chosen entropy and the resulting solution ansatz for IPM, see Appendix B.

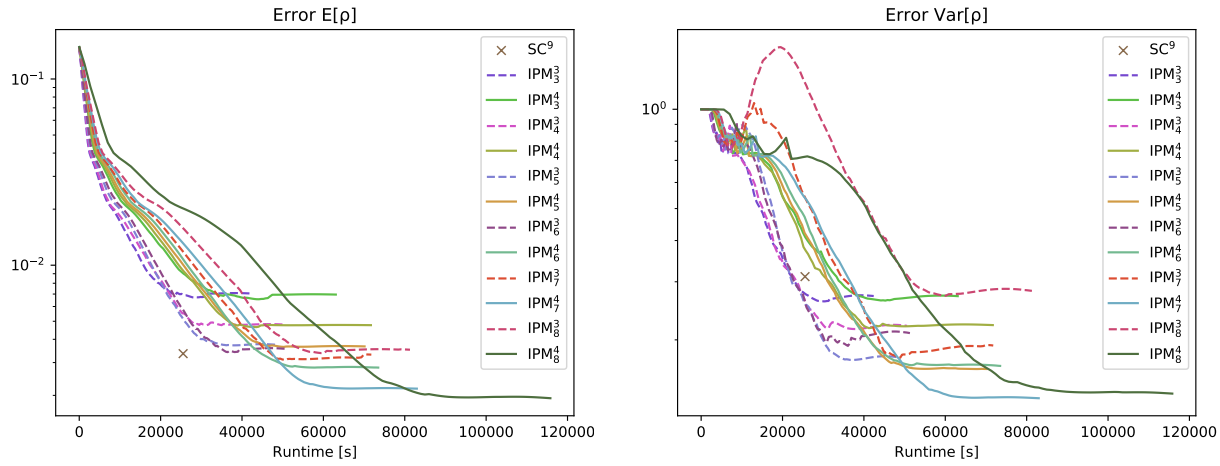

(a) (b)

Figure 2: Relative L^2 error with different quadrature levels. The subscript denotes the moment order, the superscript denotes the Clenshaw-Curtis quadrature level.

Recall that the numerical flux (9) uses a quadrature rule to approximate integrals. We start by investigating the effects this quadrature has on the solution accuracy. For this, we run the IPM method with a moment order ranging from three to seven using a Clenshaw-Curtis quadrature rule with level three (i.e. 9 quadrature points) and level four (i.e. 17 quadrature points). A comparison of the error obtained with these two quadrature levels is given in Figure 2.

- When for example comparing the error obtained with IPM_8^3 and IPM_8^4 it can be seen that the error stagnates when the chosen quadrature is not sufficiently accurate. This behavior results from aliasing

effects in the numerical flux, which dominate the accuracy level.

- If the truncation order is sufficiently small, both quadrature levels yield the same accuracy. Note that this holds for the expectation value until a truncation order of $N = 5$ and for the variance for $N = 4$. Hence, the variance is more sensitive to aliasing errors.
- Figure 2a reveals that the IPM error of $\mathrm{E}[\rho]$ with 9 quadrature points stagnates at the error level of SC^9, whereas the error of the variance in Figure 2b shows that IPM with 9 quadrature points yields an improved variance results over SC^9 even with only four moments. Hence, the number of moments needed for IPM to obtain a certain variance error is significantly smaller than the number of quadrature points needed for SC. This result can be observed throughout the results of this work. Especially for high dimensional problems, this potentially decreases the number of unknowns to reach a certain accuracy level significantly. However note, that since the numerical flux evaluation requires $O(N \cdot Q)$ operations, the numerical costs will depend on the chosen quadrature rule.

Let us now compare stochastic-Collocation with stochastic-Galerkin and IPM as well as its proposed acceleration techniques at a fixed moment order 9. Note that since IPM generalizes SG, all proposed techniques can be used for stochastic-Galerkin as well. To account for the fact that sparse grids need to be used in high dimensional problems, we use Clenshaw-Curtis quadrature rules to compute the different solutions. Stochastic-Collocation uses quadrature levels $2, 3$ and 4, which corresponds to $5, 9$ and 17 quadrature points. All adaptive methods use gPC polynomials of order 2 to 9 (i.e. 3 to 10 moments). Order 2 uses a level 2, orders 3 to 6 use a level 3 and orders 8 and 9 use a level 4 quadrature rule. The remaining methods have been computed with a level 4 quadrature rule.

All intrusive methods are iterated until the expectation value of the density fulfills the stopping criterion (19) with $\varepsilon = 5 \cdot 10^{-6}$, however it can be seen that the error saturates already at a bigger residual. For every quadrature point, SC iterates the solution until the density reaches a certain residual level ε. We observed that the SC error requires a smaller residual level to reach a constant state and we have recorded this behavior in the following table for the SC^{17} solution.

residual ρ	5e-06	4e-06	3e-06	2e-06	1e-06	9e-07	8e-07	7e-07	6e-07	5e-07
error $\mathrm{E}[\rho]$ in e-03	1.506	1.464	1.438	1.401	1.368	1.360	1.359	1.358	1.358	1.357
error $\mathrm{Var}[\rho]$ in e-03	1.339	1.332	1.292	1.248	1.217	1.215	1.214	1.213	1.213	1.213

Hence, we can deduce that SC requires a smaller residual to converge to a steady state solution. Therefore, the results for SC^{17} will be presented for a residual of $\varepsilon = 5 \cdot 10^{-6}$ as well as a reduced residual of $\varepsilon = 10^{-6}$. Note that in the case of SC, the error cannot be recorded without violating the non-intrusive framework and adding extra costs, which is why we only plot the final error and the corresponding run time.

First, let us mention that the adaptive SG method fails, since it yields negative densities during the iteration. The standard SG method however preserves positivity of mass, energy and pressure. The change of the relative L^2 error during the iteration to the steady state has been recorded in Figure 7. When comparing intrusive methods without acceleration techniques as well as SC, the following properties stick out:

- SG comes at a heavily reduced runtime, meaning that the IPM optimization problem requires a significant computational effort.
- SG_9 shows a smaller error compared to IPM_9 for the expectation value. For the variance, we see the opposite, i.e. IPM yields a better solution approximation than SG.
- Again, intrusive methods yield improved solutions compared to SC with the same number of unknowns. Actually, the error obtained with 17 unknowns when using SC is comparable with the error obtained with 10 unknowns when using intrusive methods.

The proposed acceleration techniques show the following behavior:

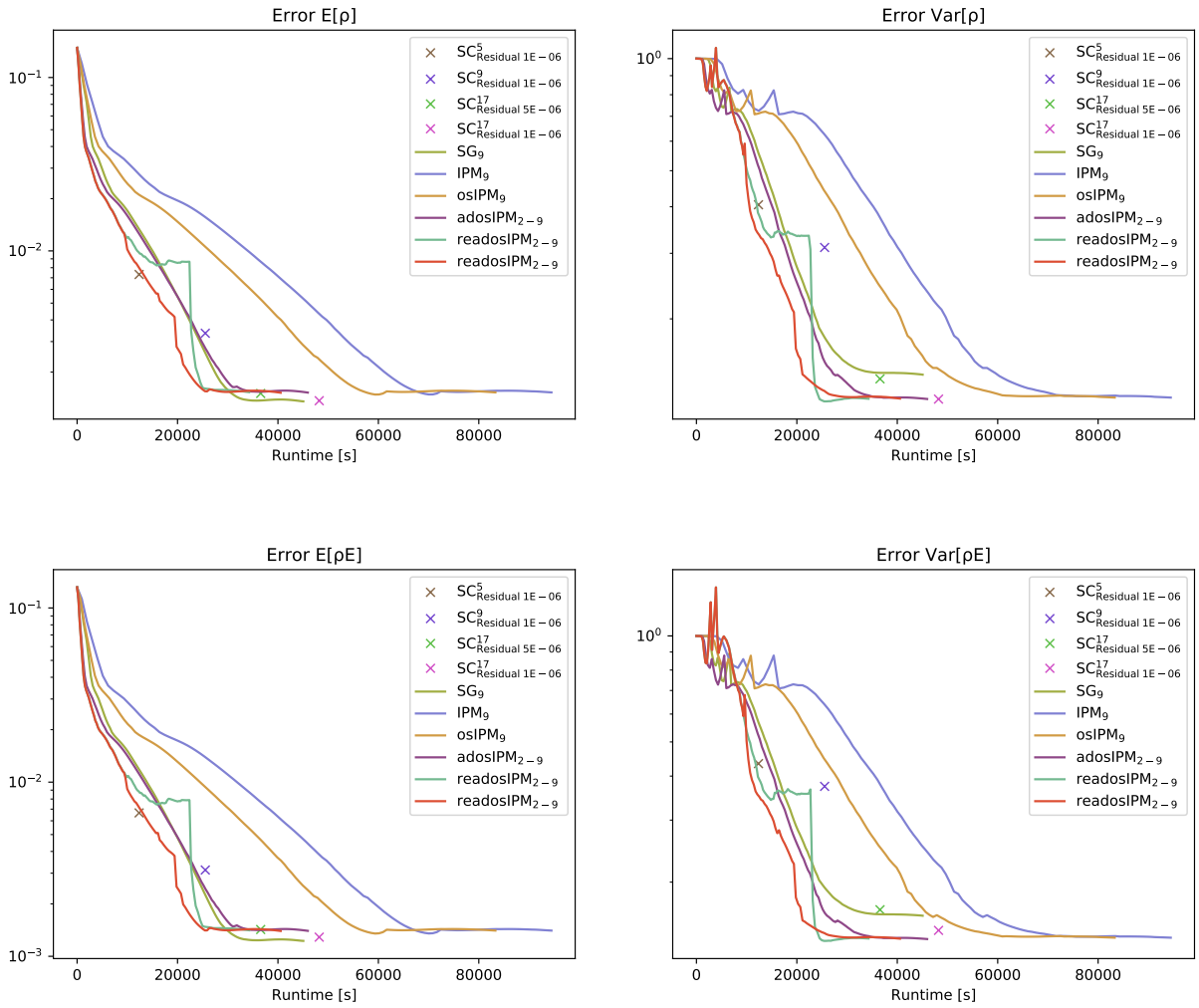

Figure 3: Relative L^2 error with 5 MPI threads for density and energy.

- The one shot IPM (osIPM) method proposed in in Section 4.2 reduces the runtime while yielding the same error as the classical IPM method.
- When using adaptivity (see Algorithm 3) in combination with the one-shot idea, the method is denoted by *adaptive one-shot IPM* (adosIPM). This method reaches the steady state IPM solution with a faster runtime than SG.
- The idea of refinement retardation combined with adosIPM (see Algorithm 4) is denoted by retardation adosIPM (readosIPM), which further decreases runtime. Here, we use two different strategies: First, we steadily increase the maximal truncation order when the residual approaches zero. To determine residual values for a given set of truncation orders $2, 4, 5$ and 8, we study at which residual level the IPM method reaches a saturated error level for each truncation order. The residual values are then determined to be $0.00006, 0.00003, 0.000022$ and 0.00002. The second, straight forward strategy converges the solution on a low truncation order of 2 to a residual of 10^{-5} and then switches to a maximal truncation order of 9. Strategy 1 is depicted in red, Strategy 2 is depicted in green. It can

be seen that both approaches reach the IPM_9 error for the same run time. Hence, we deduce that a naive choice of the refinement retardation strategy suffices to yield a satisfactory behavior.

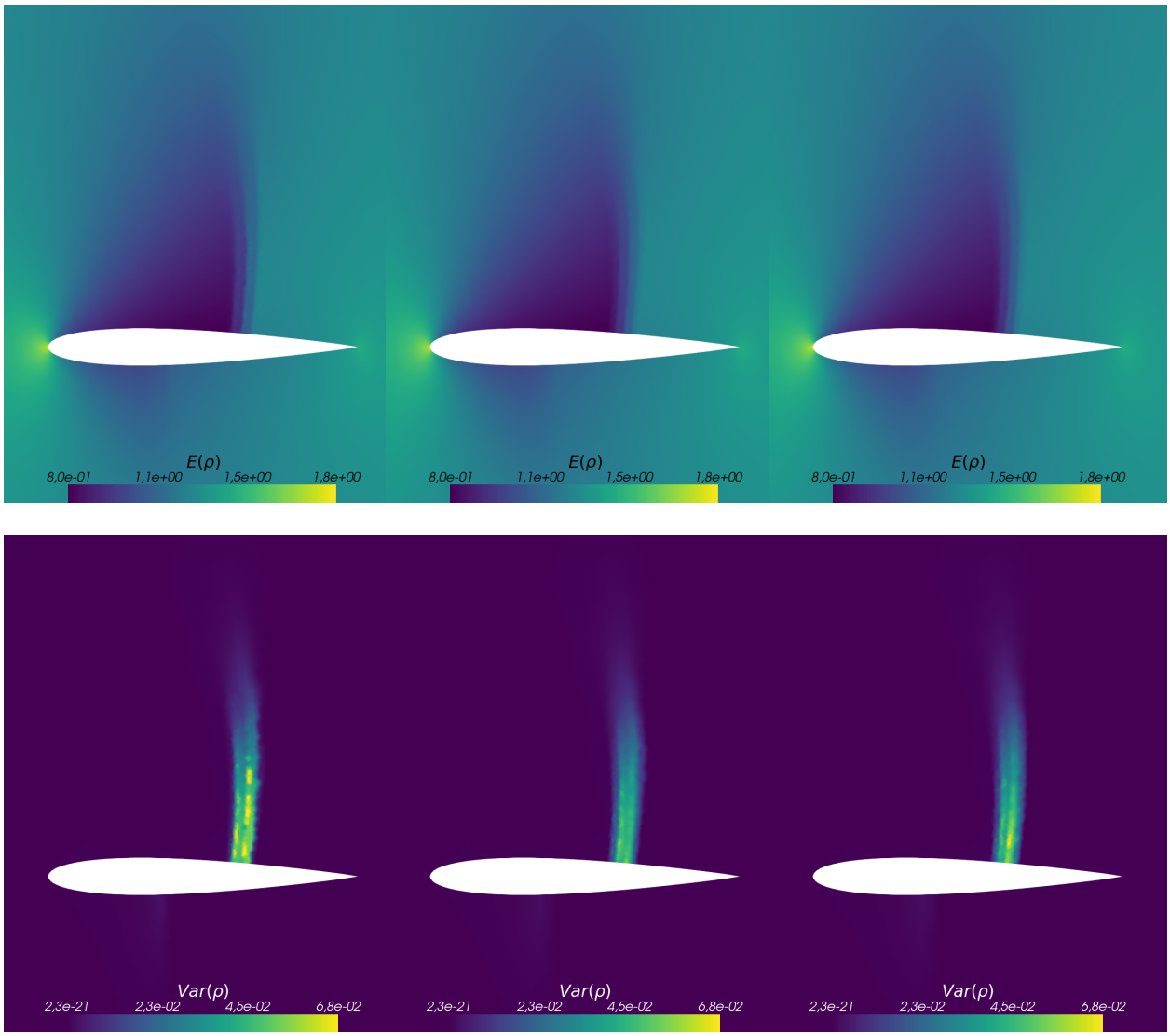

Figure 4: $\text{E}[\rho]$ and $\text{Var}[\rho]$ computed with SC^5, SG_5, IPM_5 (from left to right).

Let us finally take a look at the expectation value and variance computed with different methods. All results are depicted for a zoomed view around the airfoil. Figure 5 shows the expectation value (first row) and variance (second row) computed with 5 quadrature points for SC and 5 moments for SG and IPM. One can observe the following

- All methods yield non-physical step-like profiles of the expectation value and variance along the airfoil.
- The jump position of the intrusive solution profiles capture the exact behavior more accurately.

The readosIPM results as well as the refinement levels are depicted in Figure **??**.

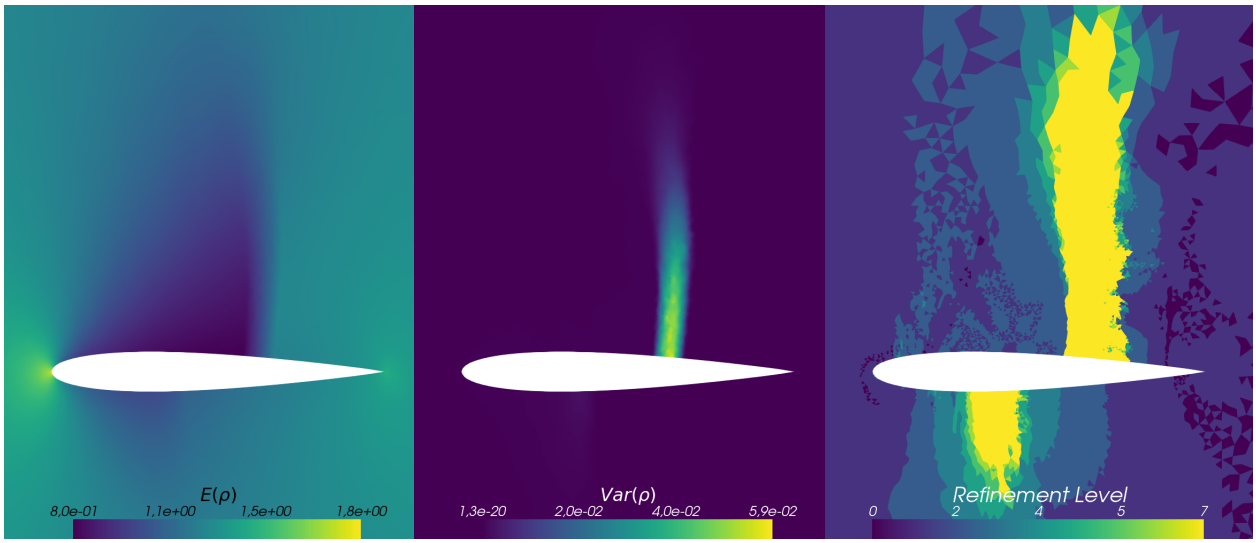

Figure 5: E[ρ], Var[ρ] and refinement level for readosIPM$_{2-9}$

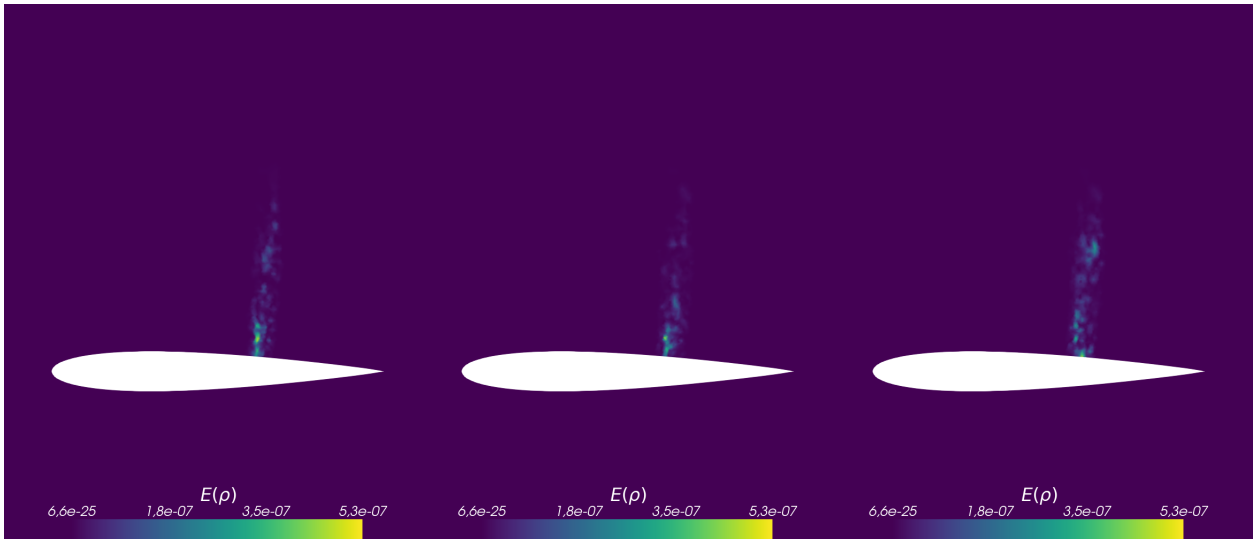

Figure 6: Errors E[ρ] for SC^{17}, SG$_{10}$, IPM$_{10}$ (from left to right).

7.2. 2D Euler equations with a two dimensional uncertainty

It sticks out that again, the intrusive methods (SG$_9$,IPM$_9$) yield a smaller error level for the same number of unknowns compared to SC. For the same number of unknowns, the run time of the intrusive methods is always bigger than the corresponding SC method. However, the error of SG and IPM lies in the area of SC^{17} at which the adaptive method has a smaller run time than SC. While SG shows a slightly better approximation of the expectation value, IPM shows a smaller error of the variance.

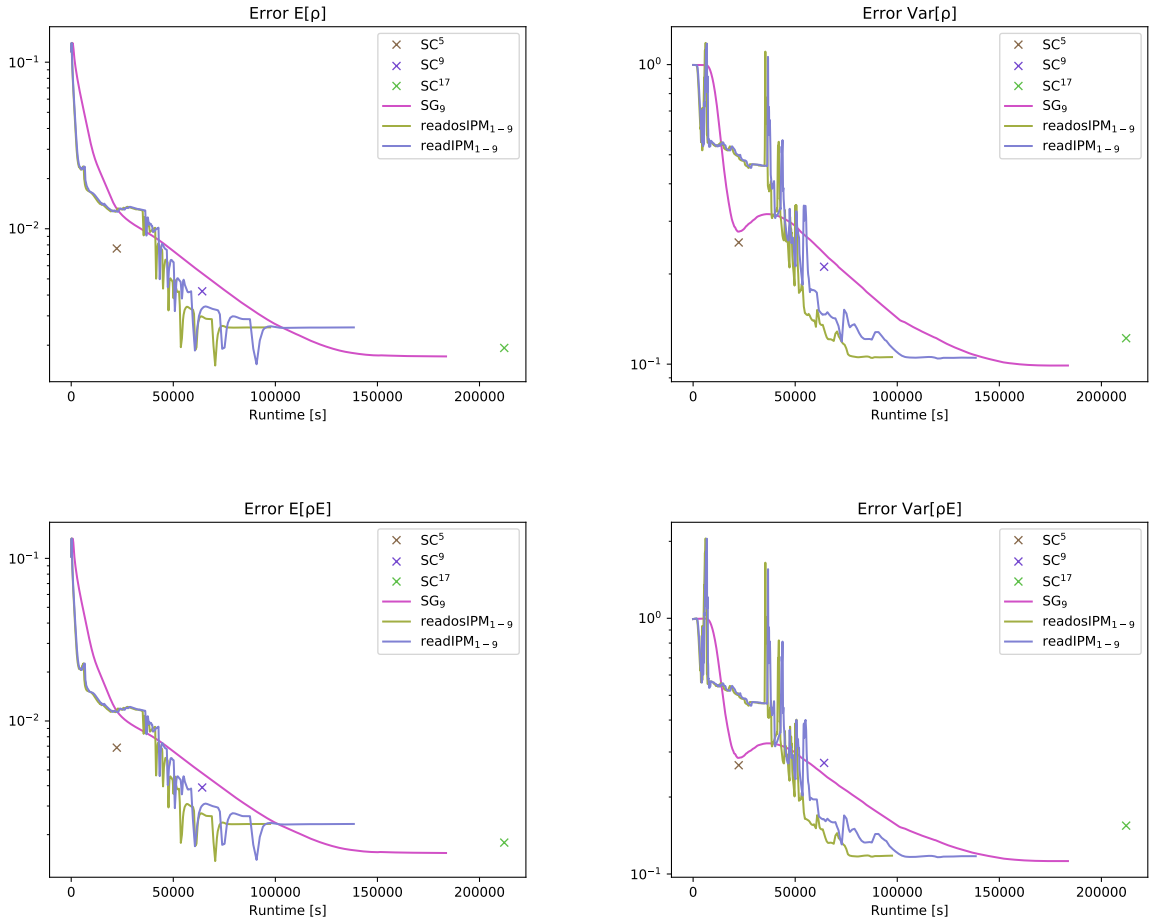

Figure 7: Relative L^2 error with 17 MPI threads for density and energy.

8. Summary and outlook

In future work, we aim at further accelerating the IPM method by using non-exact Hessian approximations. Similar to the one-shot idea of not fully converging the dual problem, it seems to be plausible to not spend too much time on computing the Hessian when the moments are not close to steady state. Hessian approximations that can be interesting are BFGS and sparse BFGS, which construct the Hessian from previously computed gradients. Note that this strategy will increase the used memory, since old Hessians or gradients from a certain number of old time steps need to be saved in every spacial cell. Even though the non-intrusive nature of stochastic-Collocation or Monte Carlo methods allows an easy implementation, it can be important to intrusively modify the code in order to fully exploit all acceleration potentials. Synchronizing the time updates of the solution at different quadrature points yields an increased control over the solution during the computation, which can for example be uses to employ adaptive methods. In this case one can switch to a fine quadrature level in a certain spatial cell by for example computing moments with the given coarse set of collocation points. From these moments one can compute an IPM reconstruction, which one can then evaluate at a finer quadrature set. Another example of breaking up the non-intrusive nature of Monte Carlo methods can be found in [30], where the generation of random samples is combined with the sampling after collisions to increase efficiency.

Appendix A. Costs of evaluating the numerical flux

In the following, we briefly discuss the number of operations needed when precomputing integrals versus the use of a kinetic flux for Burgers' equation. The stochastic Burgers' equation reads

$$\partial_t u + \partial_x \frac{u^2}{2} = 0,$$
$$u(t=0,x,\xi) = u_{IC}(x,\xi).$$

The scalar random variable ξ is uniformly distributed in the interval $[-1,1]$, hence the gPC basis functions $\boldsymbol{\varphi} = (\varphi_0, \cdots, \varphi_M)^T$ are the Legendre polynomials. Choosing the SG ansatz (3) and testing with the gPC basis functions yields the SG moment system

$$\partial_t \hat{u}_i + \partial_x \frac{1}{2} \sum_{n,m=0}^{M} \hat{u}_n \hat{u}_m \langle \varphi_n \varphi_m \varphi_i \rangle = 0.$$

Defining the matrices $\boldsymbol{C}_i := \langle \boldsymbol{\varphi}\boldsymbol{\varphi}^T \varphi_i \rangle \in \mathbb{R}^{N\times N}$ gives

$$\partial_t \hat{\boldsymbol{u}} + \partial_x \boldsymbol{F}(\hat{\boldsymbol{u}}) = 0$$

with $F_i(\hat{\boldsymbol{u}}) = \frac{1}{2}\hat{\boldsymbol{u}}^T \boldsymbol{C}_i \hat{\boldsymbol{u}}$. Note that $\boldsymbol{C}_i$ can be computed analytically, hence choosing a Lax-Friedrichs flux

$$G_i^{(LF)}(\hat{\boldsymbol{u}}_\ell, \hat{\boldsymbol{u}}_r) = \frac{1}{4}\left(\hat{\boldsymbol{u}}_\ell^T \boldsymbol{C}_i \hat{\boldsymbol{u}}_\ell + \hat{\boldsymbol{u}}_r^T \boldsymbol{C}_i \hat{\boldsymbol{u}}_r\right) - \frac{\Delta x}{2\Delta t}(\hat{\boldsymbol{u}}_r - \hat{\boldsymbol{u}}_\ell)_i \tag{A.1}$$

requires no integral evaluations. Recall, that the numerical flux choice made in this work gives

$$\boldsymbol{G}(\hat{\boldsymbol{u}}_\ell, \hat{\boldsymbol{u}}_r) = \sum_{k=1}^{Q} w_k g(\mathcal{U}(\hat{\boldsymbol{u}}_\ell;\xi_k), \mathcal{U}(\hat{\boldsymbol{u}}_r;\xi_k)) \boldsymbol{\varphi}(\xi_k) f_\Xi(\xi_k), \tag{A.2}$$

where $\mathcal{U}$ is the SG ansatz (3). When the chosen deterministic flux g is Lax-Friedrichs, the order of the polynomials inside the sum is $3M = 3(N-1)$. Choosing a Gauss-Lobatto quadrature rule, $Q = \frac{3}{2}N - 1$ quadrature points suffice for an exact computation of the numerical flux. Indeed, with this choice of quadrature points, the numerical fluxes (A.1) and (A.2) are equivalent. Counting the number of operations, one observes that our choice of the numerical flux (A.2) is significantly cheaper: When computing and storing the values in a matrix $\boldsymbol{A} \in \mathbb{R}^{Q\times N}$ with entries $a_{ki} = \varphi_i(\xi_k)$ before running the program, the numerical flux (A.2) can be split into two parts. First, we determine the SG solution at all quadrature points, i.e. we compute $\boldsymbol{u}^{(\ell)} := \boldsymbol{A}\hat{\boldsymbol{u}}_\ell$ and $\boldsymbol{u}^{(r)} := \boldsymbol{A}\hat{\boldsymbol{u}}_r$ which requires $O(N \cdot Q)$ operations. These solution values are then used to compute the numerical flux

$$G_i(\hat{\boldsymbol{u}}_\ell, \hat{\boldsymbol{u}}_r) = \sum_{k=1}^{Q} w_k g(u_k^{(\ell)}, u_k^{(r)}) a_{ki} f_\Xi(\xi_k),$$

which again requires $O(N\cdot Q)$ operations, i.e. the costs are $O(N^2)$. The evaluation of (A.1) however requires $O(N^3)$ operations.

Appendix B. IPM for the 2D Euler equations

In the following, we provide details on the implementation of IPM for the 2D Euler equations. We for clarity, we denote the momentum by $m_1 := \rho v_1$ and $m_2 := \rho v_2$ and the energy by $E := \rho e$. Then, the vector of conserved variables is $\boldsymbol{u} = (\rho, m_1, m_2, E)^T$. The entropy used is

$$s(\boldsymbol{u}) = -\rho \ln\left(\rho^{-\gamma}\left(E - \frac{m_1^2 + m_2^2}{2\rho}\right)\right).$$

Now the gradient of the entropy $\nabla_{\boldsymbol{u}} s$ has the components

$$\begin{aligned}
\frac{\partial s}{\partial \rho} &= -\ln\left(\rho^{-\gamma}\left(E - \frac{m_1^2 + m_2^2}{2\rho}\right)\right) + \frac{m_1^2 + m_2^2}{-2\rho E + m_1^2 + m_2^2} + \gamma, \\
\frac{\partial s}{\partial m_i} &= -\frac{2\rho m_i}{-2\rho E + m_1^2 + m_2^2}, \\
\frac{\partial s}{\partial E} &= -\frac{1}{\rho}\left(E - \frac{m_1^2 + m_2^2}{2\rho}\right).
\end{aligned}$$

To compute $\boldsymbol{u}_s(\boldsymbol{\Lambda}) = (\nabla_{\boldsymbol{u}} s)^{-1}(\boldsymbol{\Lambda})$, we set $\boldsymbol{\Lambda} = \nabla_{\boldsymbol{u}} s(\boldsymbol{u})$ and rearrange with respect to $\boldsymbol{u}$. Let us define

$$\alpha(\boldsymbol{\Lambda}) := \exp\left(\frac{\Lambda_2^2 + \Lambda_3^2 - 2\Lambda_1\Lambda_4 - 2\Lambda_4\gamma}{2\Lambda_4(1-\gamma)}\right) \cdot (-\Lambda_4)^{\frac{1}{1-\gamma}}$$

Then the solution ansatz $\boldsymbol{u}_s$ is given by

$$\begin{aligned}
&\rho(\boldsymbol{\Lambda}) = \alpha(\boldsymbol{\Lambda}), \qquad m_1(\boldsymbol{\Lambda}) = -\frac{\Lambda_2\alpha(\boldsymbol{\Lambda})}{\Lambda_4}, \qquad m_2(\boldsymbol{\Lambda}) = -\frac{\Lambda_3\alpha(\boldsymbol{\Lambda})}{\Lambda_4}, \\
&E(\boldsymbol{\Lambda}) = -\frac{\alpha(\boldsymbol{\Lambda})(-\Lambda_2^2 - \Lambda_3^2 + 2\Lambda_4)}{2\Lambda_4^2}.
\end{aligned}$$

References

[1] Norbert Wiener. The homogeneous chaos. *American Journal of Mathematics*, 60(4):897–936, 1938.

[2] Dongbin Xiu and George Em Karniadakis. The Wiener–Askey polynomial chaos for stochastic differential equations. *SIAM journal on scientific computing*, 24(2):619–644, 2002.

[3] Dongbin Xiu and Jan S Hesthaven. High-order collocation methods for differential equations with random inputs. *SIAM Journal on Scientific Computing*, 27(3):1118–1139, 2005.

[4] Ivo Babuška, Fabio Nobile, and Raul Tempone. A stochastic collocation method for elliptic partial differential equations with random input data. *SIAM Journal on Numerical Analysis*, 45(3):1005–1034, 2007.

[5] GJA Loeven and H Bijl. Probabilistic collocation used in a two-step approach for efficient uncertainty quantification in computational fluid dynamics. *Computer Modeling in Engineering & Sciences*, 36(3):193–212, 2008.

[6] Roger G Ghanem and Pol D Spanos. *Stochastic finite elements: a spectral approach*. Courier Corporation, 2003.

[7] Gaël Poëtte, Bruno Després, and Didier Lucor. Uncertainty quantification for systems of conservation laws. *Journal of Computational Physics*, 228(7):2443–2467, 2009.

[8] Jonas Kusch, Graham W Alldredge, and Martin Frank. Maximum-principle-satisfying second-order Intrusive Polynomial Moment scheme. *SMAI-Journal of Computational Mathematics*, 5:23–51, 2019.

[9] C. Kristopher Garrett, Cory Hauck, and Judith Hill. Optimization and large scale computation of an entropy-based moment closure. *Journal of Computational Physics*, 302:573–590, 2015.

[10] OP Le Maıtre, OM Knio, HN Najm, and RG Ghanem. Uncertainty propagation using Wiener–Haar expansions. *Journal of computational Physics*, 197(1):28–57, 2004.

[11] Jonas Kusch, Ryan G McClarren, and Martin Frank. Filtered Stochastic Galerkin Methods For Hyperbolic Equations. *arXiv preprint arXiv:1808.00819*, 2018.

[12] Timothy Barth. Non-intrusive uncertainty propagation with error bounds for conservation laws containing discontinuities. In *Uncertainty quantification in computational fluid dynamics*, pages 1–57. Springer, 2013.

[13] Richard P Dwight, Jeroen AS Witteveen, and Hester Bijl. Adaptive uncertainty quantification for computational fluid dynamics. In *Uncertainty Quantification in Computational Fluid Dynamics*, pages 151–191. Springer, 2013.

[14] Per Pettersson, Gianluca Iaccarino, and Jan Nordström. Numerical analysis of the Burgers' equation in the presence of uncertainty. *Journal of Computational Physics*, 228(22):8394–8412, 2009.

[15] Philipp Öffner, Jan Glaubitz, and Hendrik Ranocha. Stability of correction procedure via reconstruction with summation-by-parts operators for Burgers' equation using a polynomial chaos approach. *arXiv preprint arXiv:1703.03561*, 2017.

[16] Xiaoliang Wan and George Em Karniadakis. Multi-element generalized polynomial chaos for arbitrary probability measures. *SIAM Journal on Scientific Computing*, 28(3):901–928, 2006.

[17] Jakob Dürrwächter, Thomas Kuhn, Fabian Meyer, Louisa Schlachter, and Florian Schneider. A hyperbolicity-preserving discontinuous stochastic Galerkin scheme for uncertain hyperbolic systems of equations. *arXiv preprint arXiv:1805.10177*, 2018.

[18] Julie Tryoen, O Le Maıtre, and Alexandre Ern. Adaptive anisotropic spectral stochastic methods for uncertain scalar conservation laws. *SIAM Journal on Scientific Computing*, 34(5):A2459–A2481, 2012.

[19] Ilja Kröker and Christian Rohde. Finite volume schemes for hyperbolic balance laws with multiplicative noise. *Applied Numerical Mathematics*, 62(4):441–456, 2012.

[20] Jan Giesselmann, Fabian Meyer, and Christian Rohde. A posteriori error analysis for random scalar conservation laws using the Stochastic Galerkin method. *arXiv preprint arXiv:1709.04351*, 2017.

[21] Dongbin Xiu. Fast numerical methods for stochastic computations: a review. *Communications in computational physics*, 5(2-4):242–272, 2009.

[22] AK Alekseev, IM Navon, and ME Zelentsov. The estimation of functional uncertainty using polynomial chaos and adjoint equations. *International Journal for numerical methods in fluids*, 67(3):328–341, 2011.

[23] SB Hazra, V Schulz, J Brezillon, and NR Gauger. Aerodynamic shape optimization using simultaneous pseudo-timestepping. *Journal of Computational Physics*, 204(1):46–64, 2005.

[24] Bert J Debusschere, Habib N Najm, Philippe P Pébay, Omar M Knio, Roger G Ghanem, and Olivier P Le Maıtre. Numerical challenges in the use of polynomial chaos representations for stochastic processes. *SIAM journal on scientific computing*, 26(2):698–719, 2004.

[25] Jingwei Hu, Shi Jin, and Dongbin Xiu. A stochastic galerkin method for hamilton–jacobi equations with uncertainty. *SIAM Journal on Scientific Computing*, 37(5):A2246–A2269, 2015.

[26] Jingwei Hu and Shi Jin. A stochastic galerkin method for the boltzmann equation with uncertainty. *Journal of Computational Physics*, 315:150–168, 2016.

[27] J Tryoen, O Le Maitre, M Ndjinga, and A Ern. Instrusive projection methods with upwinding for uncertain non-linear hyperbolic systems. *Preprint*, 2010.

[28] Roger Ghanem and S Dham. Stochastic finite element analysis for multiphase flow in heterogeneous porous media. *Transport in porous media*, 32(3):239–262, 1998.

[29] Per-Olof Persson and Jaime Peraire. Sub-cell shock capturing for discontinuous galerkin methods. In *44th AIAA Aerospace Sciences Meeting and Exhibit*, page 112, 2006.

[30] Gaël Poëtte. A gpc-intrusive monte-carlo scheme for the resolution of the uncertain linear boltzmann equation. *Journal of Computational Physics*, 385:135–162, 2019.